Journal of Medicinal Chemistry

Article

pubs.acs.org/jmc

Pd-Catalyzed Direct C–H Bond Functionalization of Spirocyclic σ_1 Ligands: Generation of a Pharmacophore Model and Analysis of the Reverse Binding Mode by Docking into a 3D Homology Model of the σ_1 Receptor

Christina Meyer,[†] Dirk Schepmann,[†] Shuichi Yanagisawa,[‡] Junichiro Yamaguchi,[‡] Valentina Dal Col,[§] Erik Laurini,[§] Kenichiro Itami,*[,‡] Sabrina Pricl,*[,§,∥] and Bernhard Wünsch*[,†]

[†]Institut für Pharmazeutische und Medizinische Chemie der Westfälischen Wilhelms-Universität Münster, Hittorfstrasse 58-62, D-48149 Münster, Germany

[‡]Department of Chemistry, Graduate School of Science, Nagoya University, Chikusa-ku, Nagoya 464-8602, Japan

[§]Molecular Simulation Engineering (MOSE) Laboratory, Department of Industrial Engineering and Information Technology (DI3), University of Trieste, Via Valerio 10, 34127 Trieste, Italy

[∥]National Interuniversity Consortium for Material Science and Technology (INSTM), Research Unit MOSE-DEA, University of Trieste, 34127 Trieste, Italy

Supporting Information

ABSTRACT: To explore the hydrophobic binding region of the σ_1 receptor protein, regioisomeric spirocyclic thiophenes **9**–**11** were developed as versatile building blocks. Regioselective α- and β-arylation using the catalyst systems $PdCl_2$/bipy/Ag_2CO_3 and $PdCl_2$/$P[OCH(CF_3)_2]_3$/Ag_2CO_3 allowed the introduction of various aryl moieties at different positions in the last step of the synthesis. The increasing σ_1 affinity in the order **4** < **5**/**6** < **7**/**8** indicates that the positions of the additional aryl moiety and the S atom in the spirocyclic thiophene systems control the σ_1 affinity. The main features of the pharmacophore model developed for this class of σ_1 ligands are a positive ionizable group, a H-bond acceptor group, two hydrophobic moieties, and one hydrophobic aromatic group. Docking of the ligands into a σ_1 3D homology model via molecular mechanics/Poisson–Boltzmann surface area calculations led to a very good correlation between the experimentally determined and estimated free energy of receptor binding. These calculations support the hypothesis of a reverse binding mode of ligands bearing the aryl moiety at the "top" (compounds **2**, **3**, **7**, and **8**) and "left" (compounds **4**, **5**, and **6**) positions, respectively.

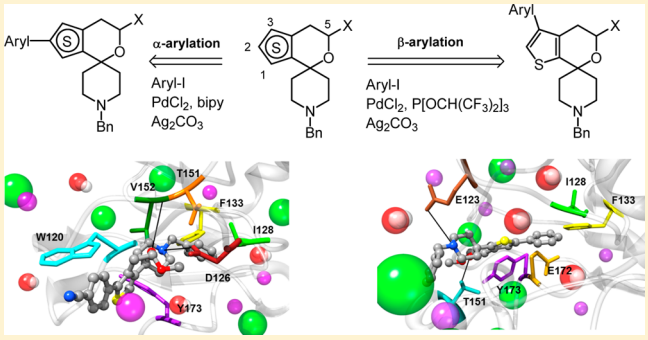

1. INTRODUCTION

The class of σ receptors consists of two subtypes, which are termed σ_1 and σ_2 receptors. Although the knowledge about the structure of the σ_2 receptor is rather low, it was reported very recently that the σ_2 receptor might be identical to the progesterone receptor membrane component 1 (pgrmc1). Cloning of pgrmc1 led to a protein of 194 amino acids with a molecular weight (MW) of 21 670.[1,2] The σ_1 receptor is well characterized on the level of DNA and amino acid sequence. The human σ_1 receptor gene encodes for a protein of 223 amino acids with a molecular weight of 25 300. The membrane-bound σ_1 receptor protein has two transmembrane domains, and both the amino and carboxy termini are located intracellularly.[3−6]

Ligands modulating the σ_1 receptor activity have a potential for the treatment of acute and chronic neurological disorders (e.g., schizophrenia, depression, (neuropathic) pain, and Alzheimer's and Parkinson's diseases). Furthermore, σ_1 antagonists are valuable drugs for the reduction of unpleasant effects after withdrawal of cocaine, methamphetamine, or alcohol from addicted animals.[7−10] Due to the high concentration of σ_1 (and σ_2) receptors in several tumor cells, σ_1 (and σ_2) ligands may be developed for the therapy and diagnosis of cancer.[11,12]

The signal transduction pathway after activation of σ_1 receptors has not been completely understood so far, and therefore, the pharmacological effects cannot be correlated with a distinct biochemical mechanism. However, involvement of σ_1 receptors in the modulation of various neurotransmitter systems (e.g., glutamatergic, dopaminergic, and cholinergic neurotransmission) has been shown. Additionally, some ion

Received: June 25, 2012
Published: August 23, 2012

channels (i.e., K^+, Na^+, and Ca^{2+} channels) are regulated by σ_1 receptors.[13−19]

Our interest has been focused on the development of novel compounds with high σ_1 receptor affinity and selectivity over related receptor systems (e.g., σ_2 receptor, phencyclidine binding site, and ifenprodil binding site of the *N*-methyl-D-aspartate (NMDA) receptor) in the central nervous system. Recently, we have shown that additional lipophilic substituents on spirocyclic σ_1 ligands favor interactions with the σ_1 receptor protein (Figure 1). Replacement of the methyl moiety of **1a** (K_i = 21 nM) with a phenyl group (**1b**, K_i = 1.5 nM) led to a 15-fold increased σ_1 receptor binding while maintaining high σ_1/σ_2 selectivity.[20,21] In the series of thiophene-annulated spirocyclic σ_1 ligands **2** and **3**, an additional aryl moiety in the α-position of the S atom is well tolerated by the σ_1 receptor protein.[22,23] These observations are in good accordance with established pharmacophore models indicating the acceptance of large lipophilic substituents by the σ_1 receptor protein.[24,25]

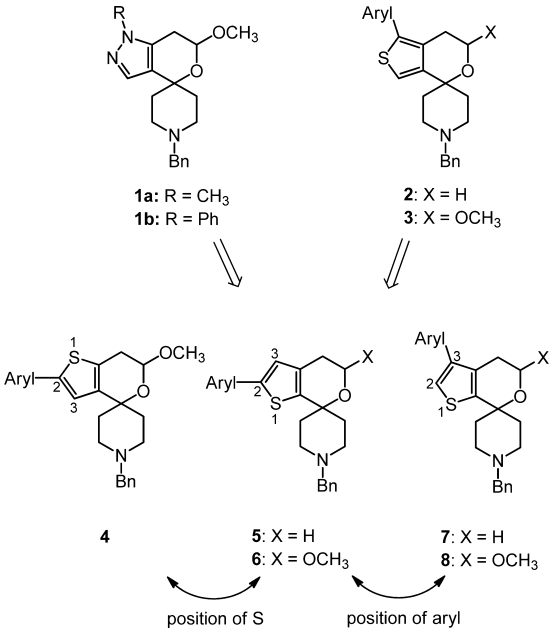

Figure 1. Design of arylated spirocyclic thiophenes.

Herein, we report on the introduction of various aryl moieties in the α-position (**4**−**6**) and β-position (**7**, **8**) of regioisomeric thiophenes by direct C−H bond arylation using recently developed Pd catalysts. Whereas the position of the additional aryl moiety of **7** and **8** correlates with the position in the lead compounds **1b**, **2**, and **3**, the aryl moiety of the spirocyclic ligands **4**−**6** is shifted to the "left" position of the thiophene ring. On the other hand, compounds **4** and **5**/**6** represent regioisomers with respect to the position of the S atom in the thiophene ring. The σ_1 affinities of the arylated thiophenes **4**−**8** are investigated in receptor binding studies with radioligands. The resulting data together with the affinity data of the arylated spirocyclic σ_1 ligands **2** and **3** are used for the establishment and validation of a σ_1 pharmacophore model. Moreover, docking of the ligands into the σ_1 receptor 3D model and affinity scoring will result in the analysis of detailed ligand receptor interactions.

2. CHEMISTRY

To obtain a large number of arylated spirocyclic thiophenes, we planned to introduce various aryl moieties into spirocyclic building blocks in the last step of the synthesis. Pd-catalyzed cross-coupling reactions of metalated arene/heteroarene and halogenated arene/heteroarene species as exemplified by the Suzuki−Miyaura coupling are undoubtedly among the most reliable methods for the synthesis of biaryls and heterobiaryls.[26] For this type of cross-coupling reaction, two activated species, i.e., a halogenated and a metalated (hetero)arene, are required. However, the direct C−H bond arylation of thiophene derivatives provides a step economical access to a large number of diverse test compounds without previous activation of the thiophene moiety.

The spirocyclic thiophene derivatives with the aryl moiety on the "left" (**4**−**6**) are obtained by α-arylation of the building blocks **9**−**11**, whereas the corresponding β-arylation of **10** and **11** provides spirocyclic compounds **7** and **8** with the aryl moiety at the "upper left" or "top" position (Figure 2).

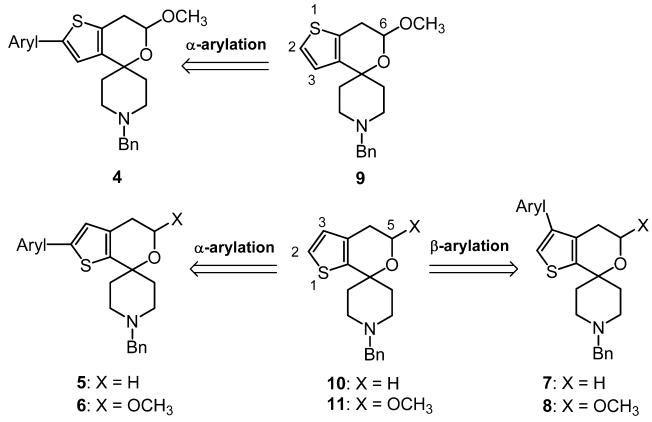

Figure 2. Plan for the synthesis of arylated spirocyclic thiophenes.

The building block **9** was synthesized as described in refs 27 and 28 beginning with the formylation of 3-bromothiophene. The synthesis of the building blocks **11** and **3a** started with (thiophen-3-yl)acetaldehyde dimethyl acetal **12** (Scheme 1), which was prepared from 3,4-dibromothiophene.[22] Halogen metal exchange with *n*-BuLi and subsequent trapping of the resulting aryllithium intermediate with 1-benzylpiperidin-4-one led to the regioisomeric hydroxy acetals **13** and **14**. After separation of both hydroxy acetals **13** and **14**, *p*-toluenesulfonic acid in methanol catalyzed the intramolecular transacetalization to form the spirocyclic thiophenes **11** and **3a**.[22]

Formation of the hydroxy acetal **13** is explained by wandering of lithium to the more stable α-position. This isomerization is strongly dependent on the temperature and the solvent used. Conducting this reaction in Et_2O at −78 °C gave exclusively the hydroxy acetal **14**. However, changing the solvent from Et_2O to tetrahydrofuran (THF) or raising the temperature to −50 or 0 °C resulted in increasing formation of the rearranged product **13**. The highest yield (41%) of the spirocyclic thiophene derivative **11** was obtained by performing the halogen metal exchange in THF at 0 °C and subsequent treatment of the mixture of hydroxy acetals **13** and **14** with *p*-toluenesulfonic acid in methanol.

The cyclic hemiacetal **15** was prepared by hydrolysis of the hydroxy acetal **13** with diluted HCl (Scheme 2). Methane-

dx.doi.org/10.1021/jm300894h | J. Med. Chem. 2012, 55, 8047−8065

Scheme 1. Preparation of Building Blocks 11 and 3a[a]

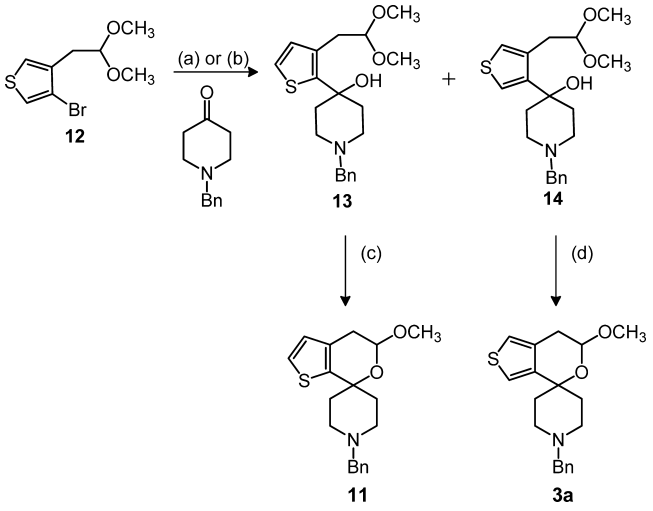

[a]Reagents and reaction conditions: (a) *n*-BuLi, THF, −78 °C, 15 min, then 1-benzylpiperidin-4-one, −78 °C, 3 h, 12% (**13**), 53% (**14**); (b) *n*-BuLi, Et_2O, 0 °C, 15 min, then 1-benzylpiperidin-4-one, 0 °C, 3 h, 33% (**13**), 17% (**14**); (c) *p*-$TolSO_3H$, CH_3OH, rt, 24 h, 54%; (d) *p*-$TolSO_3H$, CH_3OH, rt, 24 h, 51%.

Scheme 2. Preparation of Building Block 10[a]

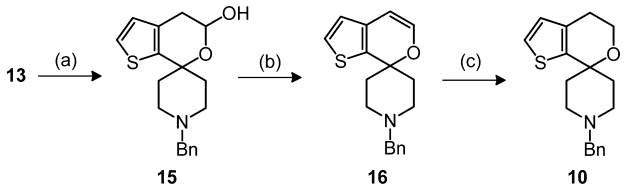

[a]Reagents and reaction conditions: (a) HCl, THF, rt, 18 h, 30%; (b) CH_3SO_2Cl, NEt_3, CH_2Cl_2, rt, 2 h, then reflux, 1 h, 67%; (c) H_2, Pd/C, CH_3OH, rt, 18 h, 67%.

sulfonyl chloride and triethylamine were used for the elimination of water from lactol **15**, providing the cyclic enol ether **16**, which was hydrogenated in the presence of the catalyst Pd/C to give the thienopyran **10**.

In 1990 Ohta and co-workers described for the first time the Pd-catalyzed direct C−H bond arylation of thiophenes with haloarenes.[29] Since this pioneering work, various catalysts based on Pd,[30] Rh,[31,32] Ir,[33] and Cu[34] have been developed for the direct arylation of nonactivated thiophene derivatives with haloarenes. These arylations typically occur in the α-position of the thiophene moiety.

In view of high α-regioselectivity, operational simplicity, and broad substrate scope, we decided to use the catalytic system $PdCl_2$/2,2′-bipyridyl/Ag_2CO_3[35,36] for the selective α-arylation of spirocyclic thiophenes **9**−**11**. To learn more about the scope of the catalytic system as well as the influence of the electron density of the additional aryl moiety on the σ_1 affinity, electron-rich and electron-poor aryl iodides were considered for the arylation step.

The results of the α-arylation of the spirocyclic thiophene **9** with different aryl iodides are summarized in Table 1. Both donor (e.g., OCH_3) and acceptor (e.g., CN) substituted aryl iodides provided the corresponding α-arylated products **4b** and **4c** in yields similar to that of the α-arylated product provided by the unsubstituted phenyl iodide (**4a**). Moreover, even the sterically demanding biphenyl derivative **4d** was obtained in

Table 1. α-Arylation of Spirocyclic Thieno[3,2-*c*]pyran 9 with Various Iodoarenes

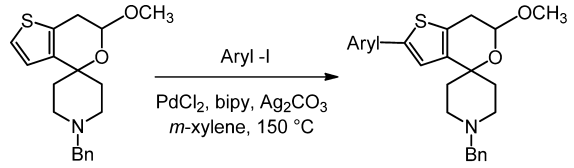

compd	aryl	yield(GPC)[a] (%)	yield(PTLC)[b] (%)
4a	C_6H_5	57	46
4b	*p*-$MeOC_6H_4$	61	38
4c	*p*-CNC_6H_4	66	53
4d	*p*-$C_6H_5C_6H_4$	67	43

[a]Yield after gel permeation chromatography. [b]Yield after preparative thin-layer chromatography.

good yields. It should be noted that these arylation conditions were well tolerated by the acid-labile methyl acetal and the basic tertiary amine of **9**.

The regioisomeric spirocyclic thiophenes **10** and **11** reacted with various aryl iodides using the same catalytic system $PdCl_2$/2,2′-bipyridyl/Ag_2CO_3 to afford the α-arylated thiophenes **5** and **6** in good yields (Table 2). Again electron-rich (e.g.,

Table 2. α-Arylation of Spirocyclic Thieno[2,3-*c*]pyrans 10 and 11 with Various Iodoarenes

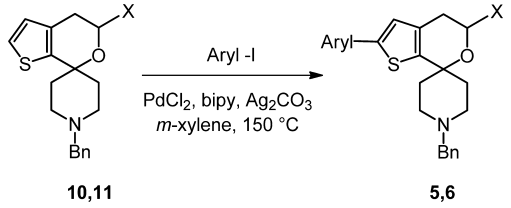

compd	X	aryl	yield(GPC)[a] (%)	yield(PTLC)[b] (%)
5a	H	C_6H_5	64	40
6a	OCH_3	C_6H_5	38	19
6b	OCH_3	*p*-$MeOC_6H_4$	51	23
6c	OCH_3	*p*-MeC_6H_4	69	52
6d	OCH_3	*p*-$NO_2C_6H_4$	61	32
6e	OCH_3	*p*-AcC_6H_4	38	29
6f	OCH_3	*p*-CNC_6H_4	55	49
6g	OCH_3	*p*-$CF_3OC_6H_4$	42	36
6h	OCH_3	1-naphthyl	63	48
6i	OCH_3	*p*-$C_6H_5C_6H_4$	97	55
6j	OCH_3	3-pyridyl	33	14

[a]Yield after gel permeation chromatography. [b]Yield after preparative thin-layer chromatography.

OCH_3, **6b**), electron-poor (e.g., NO_2, **6d**), and sterically demanding (e.g., naphthyl, **6h**) aryl iodides were employed in the last arylation step. The tertiary amino moiety, the acetalic group (**10**), and the ether group (**11**) were stable under these reaction conditions.

In addition to α-arylation, the spirocyclic systems **10** and **11** should allow the introduction of aryl moieties in the β-position. Only a few catalytic systems promoting selective β-arylation of thiophenes have been reported.[36−38] In this study the catalytic system $PdCl_2/P[OCH(CF_3)_2]_3/Ag_2CO_3$, which is easy to handle and shows high β-selectivity, was used.

dx.doi.org/10.1021/jm300894h | *J. Med. Chem.* 2012, 55, 8047−8065

The reaction of the spirocyclic thiophenes **10** and **11** with various aryl iodides led to a mixture of α-arylated (**5**, **6**) and β-arylated (**7**, **8**) products (Table 3). Therefore, the yields of the desired β-arylated spirocyclic thiophenes **7** and **8** were considerably lower than the yields of the corresponding α-substituted thiophenes **5** and **6** (compare Tables 2 and 3). In the case of β-arylation only unsubstituted and donor-substituted aryl iodides provided β-arylated products **7** and **8**. Ether (**10**), acetal (**11**), and tertiary amine did not inhibit the arylation procedure and were not decomposed by the Pd catalyst despite the high temperature of 150 °C.

Table 3. β-Arylation of Spirocyclic Thieno[2,3-*c*]pyrans 10 and 11 with Various Iodoarenes

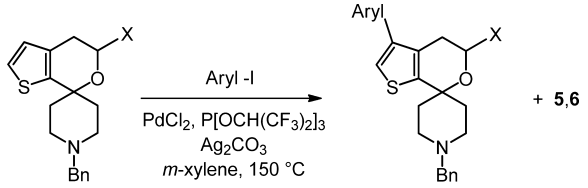

10,11 **7,8**

compd	X	aryl	yield(GPC)[a] (%)	yield(PTLC)[b] (%)
7a	H	C_6H_5	21	6
8a	OCH_3	C_6H_5	32	13
8b	OCH_3	*p*-$MeOC_6H_4$	30	15
8c	OCH_3	*p*-MeC_6H_4	57	24

[a]Yield after gel permeation chromatography. [b]Yield after preparative thin-layer chromatography.

At first, all compounds were purified by gel permeation chromatography (GPC) to isolate the arylated products. To obtain highly pure compounds (purity >95%) for receptor binding studies, the arylated products were further purified by flash chromatography (FC) or preparative thin-layer chromatography (PTLC) before testing.

3. RECEPTOR AFFINITY

The σ_1 and σ_2 receptor affinities of the arylated spirocyclic thiophenes **4**–**8**, the synthetic precursors **9**–**11**, and the lead and reference compounds were determined in competition experiments with radioligands. The potent and selective tritium-labeled radioligand [^{3}H]-(+)-pentazocine was used as a competitor for the test compounds in the σ_1 assay. Membrane preparations of guinea pig brains served as the receptor material. In the σ_2 assay, membrane preparations of rat liver

Table 4. σ_1 and σ_2 Receptor Affinities of the Spirocyclic Thiophenes and Reference Compounds

			K_i ± SEM (nM) (n = 3)		
compd	X	aryl	σ_1	σ_2	selectivity, σ_1/σ_2
1a[a]	OCH_3	CH_3	21 ± 2.3	>1 μM	>47
1b[a]	OCH_3	C_6H_5	1.5 ± 0.08	>1 μM	>660
2a[b]	H	H	0.35 ± 0.06	230	657
2b[b]	H	C_6H_5	4.5 ± 2.9	1 μM	>222
3a[b]	OCH_3	H	0.22 ± 0.06	806	3664
3b[b]	OCH_3	C_6H_5	1.0 ± 0.4	>1 μM	>1000
4a	OCH_3	C_6H_5	5.5 ± 1.5	530	96
4b	OCH_3	*p*-$MeOC_6H_4$	111 ± 27	>1 μM	>9
4c	OCH_3	*p*-CNC_6H_4	89 ± 72	>1 μM	>11
4d	OCH_3	*p*-$C_6H_4C_6H_5$	220 ± 99	>1 μM	>4
5a	H	C_6H_5	2.4 ± 0.69	283	118
6a	OCH_3	C_6H_5	16 ± 5.8	>1 μM	>63
6b	OCH_3	*p*-$MeOC_6H_4$	56 ± 23	>1 μM	>18
6c	OCH_3	*p*-MeC_6H_4	29 ± 1.0	>1 μM	>34
6d	OCH_3	*p*-$NO_2C_6H_4$	16 ± 0.9	>1 μM	>63
6e	OCH_3	*p*-AcC_6H_4	59 ± 15	>1 μM	>1
6f	OCH_3	*p*-CNC_6H_4	20 ± 6.7	>1 μM	>50
6g	OCH_3	*p*-$CF_3C_6H_4$	43 ± 18	>1 μM	>23
6h	OCH_3	1-naphthyl	12 ± 1.8	142	12
6i	OCH_3	*p*-$C_6H_4C_6H_5$	211 ± 74	>1 μM	>5
6j	OCH_3	3-pyridyl	2.5 ± 0.46	>1 μM	>400
7a	H	C_6H_5	1.6 ± 0.7	445	278
8a	OCH_3	C_6H_5	5.4 ± 0.97	>1 μM	>185
8b	OCH_3	*p*-$MeOC_6H_4$	7.1 ± 2.4	>1 μM	>141
8c	OCH_3	*p*-MeC_6H_4	2.7 ± 1.6	>1 μM	>370
9[c]	OCH_3	H	0.32 ± 0.10	>1 μM	>3000
10	H	H	1.0 ± 0.3	147	147
11	OCH_3	H	1.9 ± 0.44	>1 μM	>500
15	OH	H	16 ± 2.0	849	53
16	$C^4{=}C^5$	H	3.4 ± 1.0	236	69
haloperidol			3.9 ± 1.5	78 ± 2.0	20
di-*o*-tolylguanidine			61 ± 8	42 ± 15	0.7

[a]K_i values are reported in ref 21. [b]K_i values are reported in ref 22. [c]K_i value is reported in ref 27

dx.doi.org/10.1021/jm300894h | J. Med. Chem. 2012, 55, 8047–8065

Chart 1. Chemical Structures of the 27 Training Set Compounds

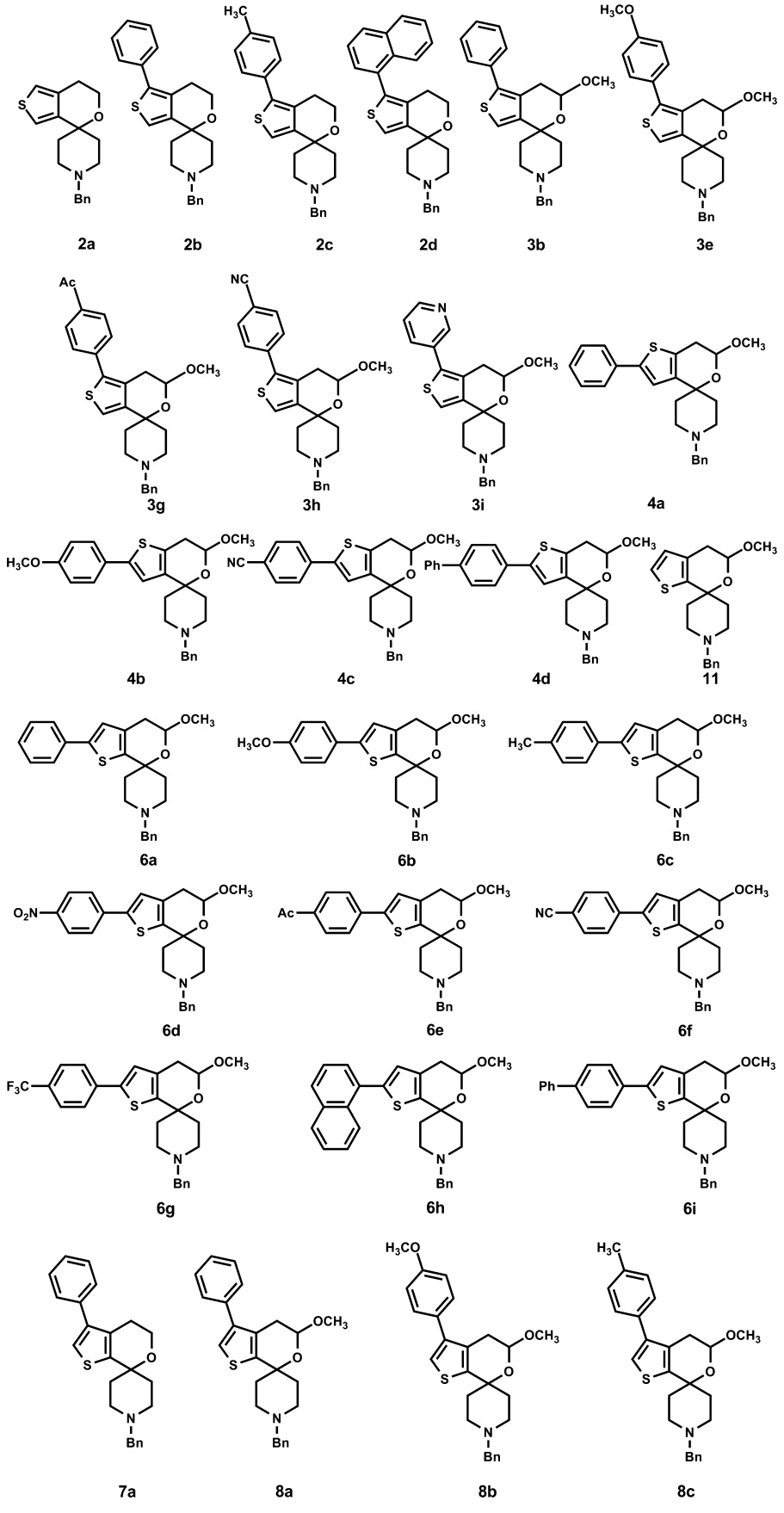

dx.doi.org/10.1021/jm300894h | J. Med. Chem. 2012, 55, 8047−8065

were the source for σ_2 receptors and [^{3}H]di-*o*-tolylguanidine was employed as a radioligand. Since di-*o*-tolylguanidine also binds to σ_1 receptors, an excess of nonradiolabeled, σ_1-selective (+)-pentazocine was added to mask σ_1 receptors.[39−42]

Table 4 clearly shows that the introduction of an aryl moiety in position 2 of the spirocyclic compound **9** bearing the S atom in the top position 1 led to a significant decrease of the σ_1 receptor affinity. The K_i values of the α-arylated compounds **4a**−**4d** are 17−500-fold higher than the K_i value of the parent thiophene **9**. The very low σ_1 affinity of the biphenylyl derivative **4d** indicates that the biphenylyl residue is sterically too demanding for the binding pocket of the σ_1 receptor.

α-Arylation of the regioisomeric thiophene derivatives **10** and **11** led to slightly reduced σ_1 affinities compared to the σ_1 affinities of their parent compounds **10** and **11**. However, some of the arylated compounds show K_i values below 20 nM (e.g., **6a**, K_i = 16 nM, **6d**, K_i = 16 nM, and **6h**, K_i = 12 nM), indicating considerable σ_1 affinities. High σ_1 affinities are achieved with either an unsubstituted aryl residue (e.g., **6a** (phenyl), K_i = 16 nM, and **6h** (naphthyl), K_i = 12 nM) or an electron-deficient aryl residue in the 2-position (e.g., **6d** (nitrophenyl), K_i = 16 nM, and **6j** (3-pyridyl), K_i = 2.5 nM). As seen for series **4**, spirocyclic thiophenes with an electron-rich aryl moiety in the 2-position gave reduced σ_1 affinities (e.g., **6b** (methoxyphenyl), K_i = 56 nM). The most promising σ_1 ligands of this series are **5a** without an acetalic methoxy group (K_i = 2.4 nM) and the 3-pyridiyl derivative **6j** (K_i = 2.5 nM) showing σ_1 affinities similar to those of the parent compounds **10** and **11**.

The highest σ_1 affinities were found for the β-arylated spirocyclic thiophenes **7** and **8**. In this compound class, even compounds with donor substituents (e.g., **8b** (methoxyphenyl), K_i = 7.1 nM; compare the K_i values of **4b** and **6b**) interact in the low nanomolar range with σ_1 receptors. Unfortunately, β-arylation of **10** and **11** with acceptor-substituted aryl iodides failed to give the arylated products.

Generally, the σ_1 affinities decreased in the order **7**/**8** > **5**/**6** > **4**. This tendency depends on the orientation of the aryl moiety. In compounds **7** and **8**, the phenyl ring adopts a position at the top of the molecule, which is favorable for receptor interaction. Due to the increased C−S bond length and the larger size of the S atom, the spirocyclic thiophenes **5** and **6** with the S atom in the "bottom" position direct the aryl moiety in a position similar to its position in **7**/**8**, whereas in the regioisomers **4** with the S atom in the top position the additional aryl moiety is directed in an unfavorable position.

Except for the naphthyl derivative **6h** and the unsubstituted compound **10**, the σ_2 affinities of the (arylated) spirocyclic thiophenes **4**−**11** are very low, indicating high selectivity for the σ_1 subtype over the σ_2 subtype. Despite the moderate σ_2 affinity of **10** (K_i = 147 nM), its σ_1/σ_2 selectivity is still high (147) due to the very high σ_1 affinity. On the contrary, the naphthyl derivative **6h** shows the lowest σ_1/σ_2 selectivity (12) within this series of compounds.

Since the antagonistic activity of similar spirocyclic piperidines has been shown in animal assays,[27,43] we assume that the new thiophene-annulated spirocyclic compounds presented herein also have antagonistic activity.

To prove the receptor selectivity, the affinities of the spirocyclic piperidines **6c**, **6f**, **6h**, **6j**, **8c**, **10**, and **11** toward the phencyclidine binding site[44] and the ifenprodil binding site[45] of the NMDA receptor were recorded. It was shown that the affinity of these very promising σ_1 ligands at these receptor systems is rather low; the K_i values are generally greater than 500 nM. This result indicates a very high selectivity of these σ_1 ligands over the phencyclidine and ifenprodil binding sites of the NMDA receptor.

4. MOLECULAR MODELING OF LIGAND/PROTEIN INTERACTIONS

To investigate the role played by the position of the aromatic moiety on the thiophene ring in determining the affinity of our compounds toward the σ_1 receptor, we applied a sequential molecular modeling procedure based on the following steps: (i) generation of a 3D pharmacophore model for the present series of compounds, (ii) 3D pharmacophore-guided docking of all ligands into the putative binding site of our 3D σ_1 receptor model, (iii) estimation of their binding affinity via the molecular mechanics/Poisson−Boltzmann surface area (MM/PBSA) methodology, and (iv) comparison with the available experimental activities.

4.1. Pharmacophore Model Generation. A pharmacophore represents the three-dimensional arrangements of structural or chemical features of a drug that may be essential for interacting with the receptor for optimal binding. These pharmacophore models can be used in different ways in drug design programs, e.g., (1) as 3D query tools in virtual screening to identify potential new compounds from 3D databases of druglike molecules with patentable structures different from those already discovered, (2) to predict the activities of a set of new compounds yet to be synthesized, or, as in the present case, (3) to understand the possible mode/mechanism of drug/receptor interaction.

3D pharmacophore hypothesis generation by the Catalyst software is one of the popular approaches that has been successfully used in drug discovery and toxicology research so far. The most critical aspect of Catalyst pharmacophore hypothesis generation is the selection of the molecular training set; however, some basic guidelines have been elegantly laid out by Li et al.,[46] among which (1) a minimum of 16 diverse compounds should be selected as a training set to avoid any chance correlation, (2) the affinity data should have a range of 4−6 orders of magnitude, (3) the most active compounds should be included so that they provide information on the most critical features required as a pharmacophore, (4) all biological data must be obtained by homogeneous procedures.

On the basis of the above criteria, a set of 10 pharmacophore hypotheses were generated with Catalyst using 27 training set compounds listed in Chart 1. The results of the hypotheses, which include different cost values calculated during hypothesis generation along with the corresponding root-mean-square deviation (rmsd), correlation coefficient (ρ), and pharmacophore features, are listed in Table 5.

The total hypothesis cost of these 10 best models varies between 122.9 bits for the best ranked model (Hypo1) and 178.9 bits for the lowest ranked one (Hypo10). Such a confined difference (56 bits) reflects both the homogeneity of the generated hypotheses and the adequacy of the molecular training set. The difference between the null and the fixed costs, which should be higher than 70 bits to guarantee a robust correlation, is 89.6 bits in our case. This corresponds to a chance of true correlation in the data greater than 90%.[47] Furthermore, in all the generated hypotheses the total costs are much closer to the fixed cost (115.7 bits) than to the null cost (205.3 bits), indicating that meaningful models are obtained. Finally, the rmsd's and the correlation coefficients (ρ) between estimated and experimental affinities range from 0.922 to 1.874

Table 5. Composition (Features), Costs (Bits), and Statistical Parameters (rmsd and ρ) Associated with the 10 Best Hypotheses (Pharmacophore Models) Generated with the Catalyst Software Using the Training Set Molecules (Chart 1)

hypothesis	total cost	Δcost[a]	rmsd	ρ	features[b]
1	122.9	82.6	0.922	0.905	HBA, HYAr, HY, HY, PI
2	131.5	73.8	1.305	0.839	HBA, HY, HY, HY, PI
3	136.4	68.9	1.319	0.832	HBA, HYAr, HY, HY, PI
4	137.8	67.5	1.377	0.813	HBA, HYAr, HYAr, HY, PI
5	139.6	65.7	1.418	0.792	HBA, HY, HY, HY, PI
6	142.8	62.5	1.490	0.775	HBA, HYAr, HY, PI
7	148.5	56.8	1.558	0.760	HBA, HY, HY, PI
8	153.4	51.9	1.704	0.739	HBA, HYAr, HYAr, PI
9	173.6	31.7	1.792	0.701	HBA, HYAr, HY, PI
10	178.9	26.4	1.874	0.695	HBA, HYAr, HY, PI

[a]Δcost = null cost − total cost. Null cost = 205.3, fixed cost = 115.7, and configurational cost = 12.5. All costs are in units of bits. [b]HBA = hydrogen bond acceptor, HYAr = hydrophobic aromatic, HY = hydrophobic, and PI = positive ionizable (see the text for more details).

and from 0.905 to 0.695, respectively. As all the generated pharmacophores map the molecules of the training set in a similar way, the first model (Hypo1), characterized by the highest cost difference, the lowest rmsd, and the best ρ value, was selected for further analysis.

In analogy with other pharmacophore models formerly developed for σ_1 ligands,[48−51] the main features of the present Hypo1 are a positive ionizable group (PI), a hydrogen bond acceptor group (HBA), two hydrophobic moieties (HY), and one hydrophobic aromatic point (HYAr) (see Figure 3).

The affinities of the 27 compounds for the σ_1 receptor estimated using Hypo1 are reported in Table 6, along with the experimental values and the relevant errors (expressed as the ratio between estimated and experimental values). Table 6 clearly shows that 21 out of 27 molecules in the training set have errors equal to or less than 2.2, while the remaining 6 have errors less than 5.0.

Pharmacophore mapping of compounds belonging to series **3** and **8**—all bearing an aromatic ring in the top position with respect to the tetrahydropyran ring—indicates that these molecules can map all five pharmacophore features quite nicely (see Figure 4). Indeed, the presence of the *N*-benzylic group provides one of the aromatic functions (HY) to the molecules, the other HY being provided by the thiophene ring. The piperidinic nitrogen atom is aptly positioned over the PI feature, the pyran ring oxygen fulfills the HBA requirement, and, last, the phenyl substituent overlays the HYAr feature independently of its α-position (**3b**) or β-position (**8a**) with respect to the heterocyclic sulfur atom. Referring to compounds **3b** and **8a** of Figure 4 as an example, the in silico estimated K_i (σ_1) values (K_i = 1.2 nM for **3b** and K_i = 3.4 nM for **8a**) are in excellent agreement with the corresponding experimentally determined K_i values (1.0 nM for **3b** and 5.4 nM for **8a**; see Table 6).

On the contrary, compounds belonging to series **4** and **6** featuring the aryl substituent in the left position are all endowed with a lower affinity toward the σ_1 receptor since all explored molecular conformations failed to access the HYAr feature, as exemplified for compounds **4a** and **6a** in Figure 5. The HYAr pharmacophore interaction point is, however, the only feature unmapped by compounds of series **4** and **6**. Thus, given the excellent overlay between the molecular chemical moieties and the remaining 3D pharmacophore requirements shown in Figure 5, only a small decrease in σ_1 affinity for these two molecular series is predicted for, e.g., compounds **4a** and

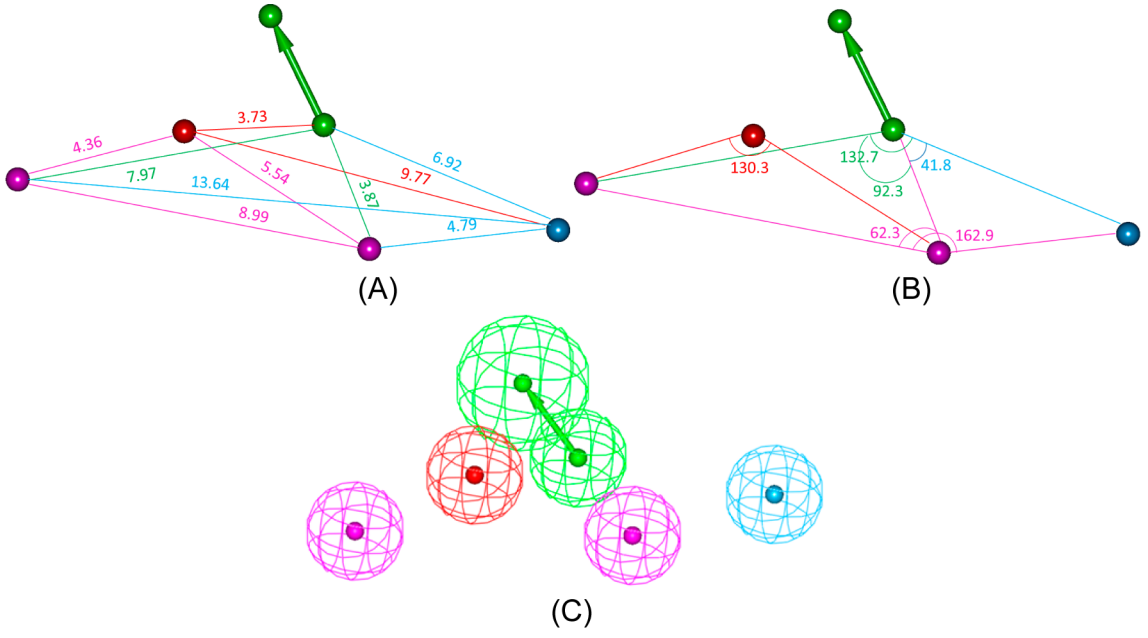

Figure 3. Geometrical relationships (A, B) among the features of the top-scoring pharmacophore Hypo1 (C). The hypothesis features are portrayed as meshed spheres, color-coded as follows: red, PI; light blue, HYAr; pink, HY; light green, HBA. HBA is actually represented as a pair of spheres (the smaller sphere represents the location of the HBA atom on the ligand and the larger one the location of an HB donor on the receptor). Selected distances (Å) and angles (deg) are labeled.

dx.doi.org/10.1021/jm300894h | J. Med. Chem. 2012, 55, 8047−8065

Table 6. Experimentally Determined and Estimated K_i Values of the Training Set Compounds Calculated on the Basis of Pharmacophore Hypothesis 1 (Hypo1)

compd of this paper	compd of ref 22	aryl	X	σ_1 affinity, K_i (nM) estimated	exptl	error[a]
	2a		H	1.8	0.35	5.0
	2b	C_6H_5	H	2.7	4.5	−1.6
	2c	*p*-MeC_6H_5	H	2.8	3.6	−1.3
	2d	1-napthyl	H	6.9	4.0	1.7
	3b	C_6H_5	$-OCH_3$	1.2	1.0	1.2
	3e	*p*-$MeOC_6H_5$	$-OCH_3$	3.1	2.2	1.4
	3g	*p*-AcC_6H_5	$-OCH_3$	3.5	1.6	2.2
	3h	*p*-CNC_6H_5	$-OCH_3$	0.51	0.25	2.0
	3i	3-pyridyl	$-OCH_3$	1.9	2.2	−1.1
4a		C_6H_5	$-OCH_3$	13	5.5	2.2
4b		*p*-$MeOC_6H_5$	$-OCH_3$	50	111	−2.2
4c		*p*-CNC_6H_5	$-OCH_3$	60	89	−1.5
4d		*p*-biphenyl	$-OCH_3$	51	220	−4.3
11			$-OCH_3$	5.7	1.9	3.0
6a		C_6H_5	$-OCH_3$	23	16	1.4
6b		*p*-$MeOC_6H_5$	$-OCH_3$	67	56	1.2
6c		*p*-MeC_6H_5	$-OCH_3$	27	29	−1.1
6d		*p*-$NO_2C_6H_5$	$-OCH_3$	51	16	3.2
6e		*p*-AcC_6H_5	$-OCH_3$	34	59	−1.7
6f		*p*-CNC_6H_5	$-OCH_3$	37	20	1.8
6g		*p*-$CF_3C_6H_5$	$-OCH_3$	21	43	−2.0
6h		1-naphthyl	$-OCH_3$	22	12	1.8
6i		*p*-biphenyl	$-OCH_3$	45	211	−4.7
7a		C_6H_5	H	1.8	1.6	1.1
8a		C_6H_5	$-OCH_3$	3.4	5.4	−1.6
8b		*p*-$MeOC_6H_5$	$-OCH_3$	2.2	7.1	−3.3
8c		*p*-MeC_6H_5	$-OCH_3$	3.5	2.7	1.3

[a]Values in the error column represent the ratio of the estimated affinity to experimental affinity, or its negative inverse if the ratio is less than 1.

6a (K_i = 13 nM for **4a** and K_i = 23 nM for **6a**), in agreement with the experimental binding constants (K_i = 5.5 nM for **4a** and K_i = 16 nM for **6a**; see Table 6).

Importantly, however, the affinity of compounds **4** and **6** is strongly affected by the presence of a substituent at the *para* position of the thiophene-linked phenyl ring. On the contrary, all derivatives **3** and **8** bearing the same substituted aromatic moieties are endowed with comparable (if not higher) σ_1 affinities with respect to the unsubstituted counterparts.

In this respect, the analysis of the top panels of Figure 6 indeed reveals how, for compounds **3e** and **8b** bearing the *p*-methoxyphenyl substituent in the top position, all five 3D pharmacophore features are mapped very well (as in the case of their unsubstituted analogues; see Figure 4), resulting in high predicted/experimental σ_1 affinity values (K_i(estimated) = 3.1 nM/K_i(exptl) = 2.2 nM for **3e** and K_i(estimated) = 2.2 nM/K_i(exptl) = 7.1 nM for **8b**; see Table 6).

On the other hand, not only do all derivatives characterized by the presence of the aromatic ring in the left position miss the HYAr feature as discussed above, but the presence of the *p*-OCH_3 substituent on the phenyl ring induces a further conformational change so that all four remaining pharmacophoric features are mapped less precisely with respect to the unsubstituted compounds (compare the lower panels in Figures 5 and 6). Accordingly, for this set of compounds the model predicts lower σ_1 affinities for **4b** (K_i = 50 nM) and **6b** (K_i = 67 nM) in line with the experimental σ_1 affinities (K_i = 111 nM for **4b** and K_i = 56 nM for **6b**; see Table 6).

4.2. Pharmacophore Assessment: Cross-Validation Study. The quality of the developed pharmacophore was assessed using the CatScramble technique available in Catalyst. The purpose of this technique is to randomize the affinity data among the training set compounds and to generate pharmacophore hypotheses using the same features and parameters used to develop the original pharmacophore hypothesis. If the randomized sets generate pharmacophores with similar or better cost values, rmsd's, and correlations, then the original pharmacophore can be considered as generated by chance. The results of the CatScramble runs are listed in Table 7. Since a 98% confidence level was selected for this test, 49 random hypothesis runs were performed. The results clearly indicate that randomization produced hypotheses with no predictive values similar or close to those of the corresponding Hypo1. Indeed, none of the outcome hypotheses had a lower cost score, better correlation, or smaller root-mean-square deviation than the initial hypothesis. Table 7 lists the first 10 lowest total score values of the resulting 49 hypotheses for our training set molecules. In conclusion, there is a 98% chance for the best hypothesis to represent a true correlation in the training set affinity data for the present classes of compounds.

Finally, a further statistical test, the *leave-one-out method*, which consists of recomputing the hypothesis by excluding from the training set one molecule at a time, was carried out. Basically, this test is performed to verify whether the correlation is strongly dependent on one particular compound in the

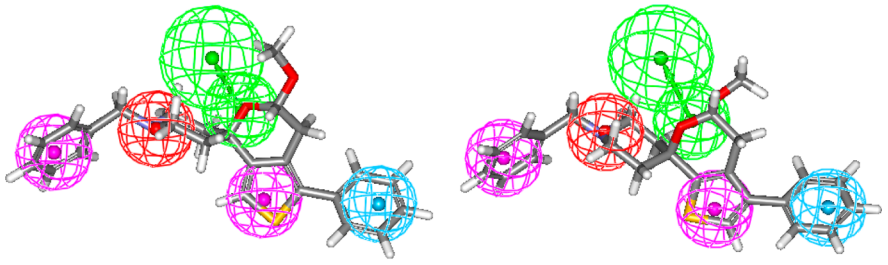

Figure 4. Mapping of compounds **3b** and **8a** onto the developed σ_1 3D pharmacophore model (Figure 3). Compounds are portrayed as atom-colored sticks (red, O; yellow, S; gray, C; blue, N; white, H).

dx.doi.org/10.1021/jm300894h | J. Med. Chem. 2012, 55, 8047−8065

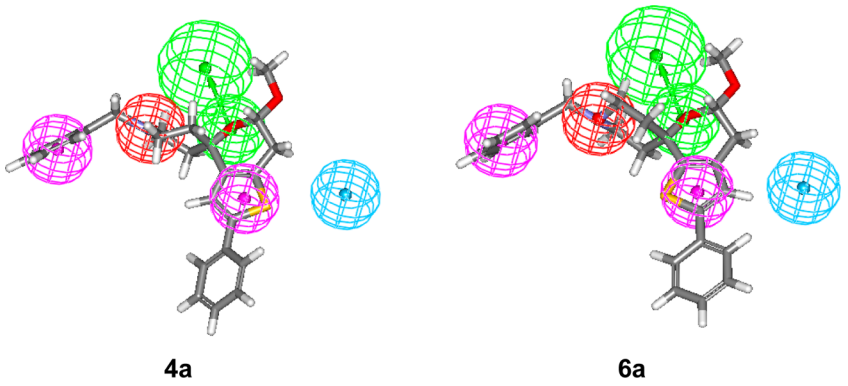

Figure 5. Mapping of compounds **4a** and **6a** onto the developed σ_1 3D pharmacophore model (Figure 3). Compounds are portrayed as atom-colored sticks (red, O; yellow, S; gray, C; blue, N; white, H).

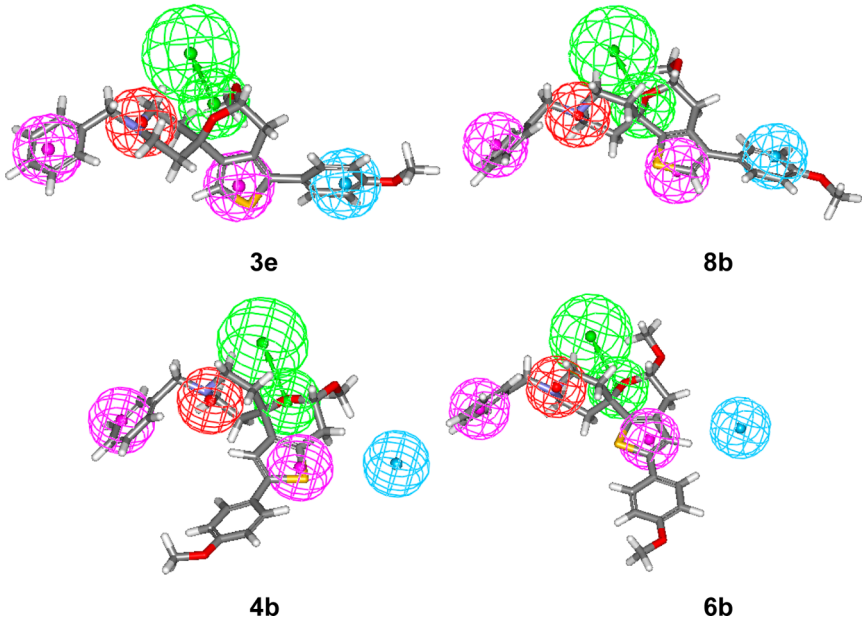

Figure 6. Mapping of compounds **3e**, **8b**, **4b**, and **6b** onto the developed σ_1 3D pharmacophore model (Figure 3). Compounds are portrayed as atom-colored sticks (red, O; yellow, S; gray, C; blue, N; white, H).

Table 7. Output Parameters of the 10 Lowest Cost Hypotheses Resulting from the Statistical Evaluation According to the CatScramble Validation Procedure

hypothesis	ρ	rmsd	total cost (bits)
1	0.812	1.154	142.9
2	0.717	1.389	151.9
3	0.700	1.397	154.0
4	0.724	1.453	155.1
5	0.622	1.496	157.1
6	0.603	1.601	160.6
7	0.576	1.657	163.8
8	0.558	1.708	165.7
9	0.515	1.755	167.8
10	0.507	1.823	168.9
Hypo1	0.905	0.922	122.9

training set. The test is positive if the affinity of each excluded molecule is correctly predicted by the corresponding one-missing hypothesis. The value of ρ, the feature composition of the pharmacophore, and the quality of the predicted affinity of the excluded molecule were used as measures for the assessment of the statistical test. For each of the 27 new hypotheses generated according to this method, we did not obtain meaningful differences between Hypo1 and each hypothesis resulting from the exclusion of one compound at a time.

4.3. Pharmacophore Validation Using Test Set Compounds. A critical step in automated pharmacophore generation is model validation, especially in those cases where the model has been generated for the purpose of either predicting the affinity of external sets of compounds or estimating the affinity of newly conceived molecular entities prior to their synthesis. Thus, to check the robustness of our correlation, we used the pharmacophore model (Hypo1) to predict the affinity of a further set of molecules, also called the test set, composed of 13 additional molecules from our series (see Chart 2).

Interestingly, a good correlation coefficient of 0.80 was observed when a regression analysis was performed by mapping the test set onto the features of the best pharmacophore hypothesis (Hypo1). The predicted and the experimental $K_i(\sigma_1)$ values for the test set along with the respective errors are shown in Table 8. The average error in predicting the affinity of

dx.doi.org/10.1021/jm300894h | J. Med. Chem. 2012, 55, 8047−8065

Chart 2. Chemical Structures of the 13 Test Set Compounds

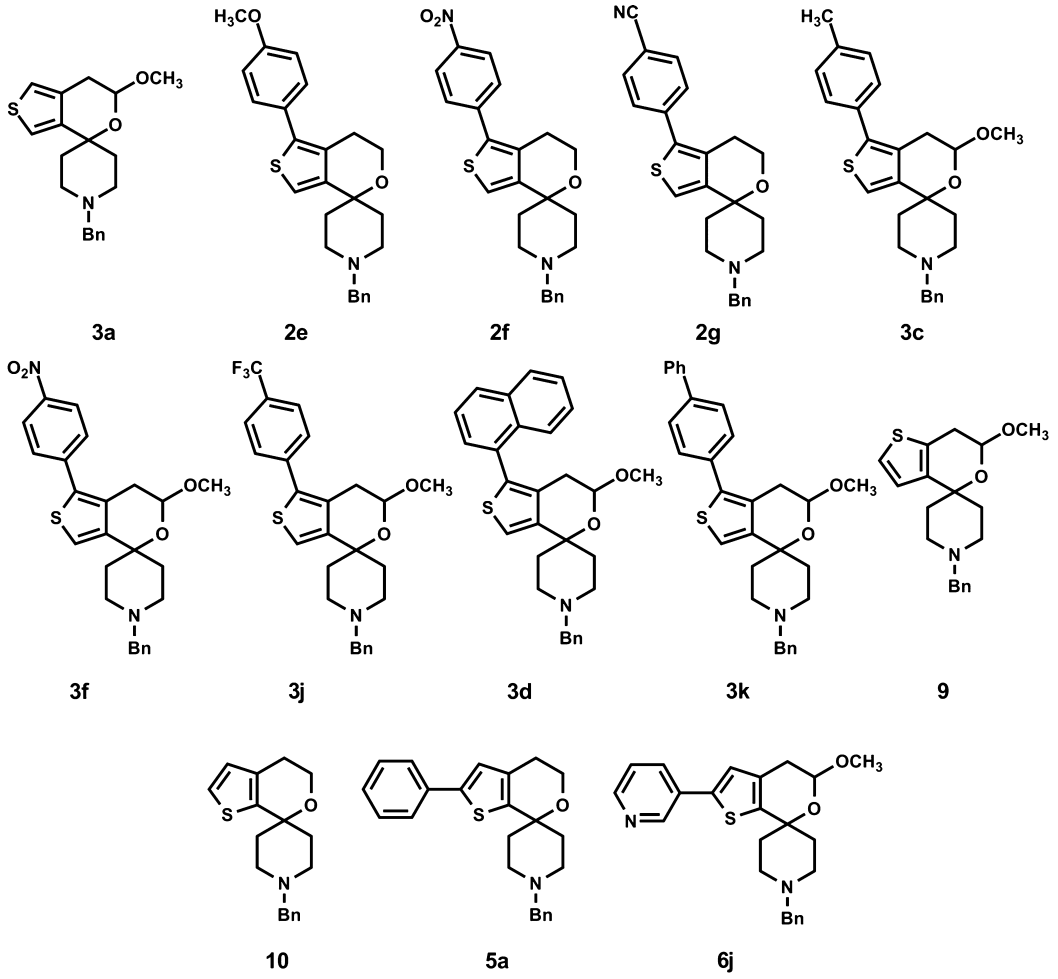

Table 8. Experimentally Determined and Estimated K_i Values of the Test Set Compounds Calculated on the Basis of Pharmacophore Hypothesis 1 (Hypo1)

compd of this paper	compd of ref 22	aryl	X	σ_1 affinity: K_i (nM) estimated	exptl	error
	3a		$-OCH_3$	1.8	0.22	7.7
	2e	*p*-$MeOC_6H_5$	H	1.6	1.5	1.1
	2f	*p*-$NO_2C_6H_5$	H	3.4	1.7	2.0
	2g	*p*-CNC_6H_5	H	2.7	3.4	−1.3
	3c	*p*-MeC_6H_5	$-OCH_3$	1.1	2.0	−1.9
	3f	*p*-$NO_2C_6H_5$	$-OCH_3$	3.6	1.0	3.6
	3j	*p*-$CF_3C_6H_5$	$-OCH_3$	2.1	5.7	−2.7
	3d	1-naphthyl	$-OCH_3$	5.8	5.0	1.2
	3k	*p*-biphenyl	$-OCH_3$	18	30	−1.7
9			$-OCH_3$	2.0	0.32	6.3
10			H	3.2	1.0	3.2
5a		C_6H_5	H	11	2.4	4.6
6j		3-pyridyl	$-OCH_3$	5.4	2.5	2.2

the test set molecules is 3.0. Given the inherent simplicity of the pharmacophoric approach, and considering the intrinsic variability of the biological responses, we can conclude that the ability of the present 3D pharmacophore model to predict the affinity of these series of σ_1 receptor ligands is quite satisfactory.

4.4. Docking of Ligands into the σ_1 Receptor 3D Model and Affinity Scoring via MM/PBSA Calculations. Following our pioneer work,[50] the putative binding site and binding modes of all compounds considered in this work in the σ_1 receptor 3D homology model structure were retrieved by exploiting the currently available preliminary information on sequence−structure relationships and mutagenesis studies[52] and the ligand-binding pharmacophore requirements presented above.[50,51] To summarize briefly, a protein isoform missing residues 119−149 was found devoid of ligand-binding capacity, and the conversion of residues Asp126 and Glu172 into glycine led to a several-fold reduction in ligand binding of the σ_1 receptor.[52] Moreover, our hydrophobicity analysis[50] identified, aside for the TM regions, a third hydrophobic region matching the SBDLII (steroid binding domain like II) region and centered on Asp188, a residue specifically photolabeled by [^{125}I]IACoc (3-iodo-4-azidococaine).[53,54] Having localized this protein region as a possible zone for ligand binding, a thorough search for a sequence satisfying the chemical features imposed by Hypo1 was performed, and the sequence was successfully retrieved. Thus, all compounds were docked into the putative binding site of the receptor 3D model. In the set of docked ligand conformations, for each compound a solution was found that best reproduced the key 3D pharmacophore requirements.

Taking compound **3h** as a prototypical example of the class of compounds featuring the phenyl ring in the top position, from the top panel of Figure 7, we can observe the striking

dx.doi.org/10.1021/jm300894h | J. Med. Chem. 2012, 55, 8047−8065

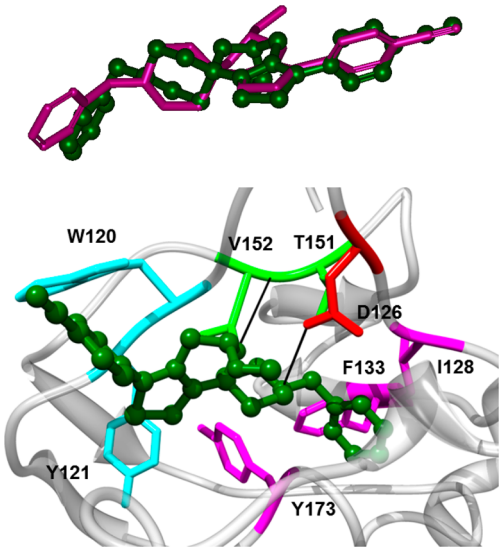

Figure 7. (Top) Comparison between the best conformation assumed by compound **3h** upon mapping the 3D pharmacophore model (purple sticks) and after docking in the putative σ_1 binding site (green sticks and balls). (Bottom) Equilibrated MD snapshots of the σ_1 receptor in complex with **3h**. The image is a zoomed view of the receptor binding site. The ligand is portrayed in green sticks and balls, while the protein residues mainly involved in the interaction with **3h** are highlighted as colored sticks and labeled. Salt bridge and H-bond interactions are shown as black lines. Water, ions, and counterions are not shown for clarity.

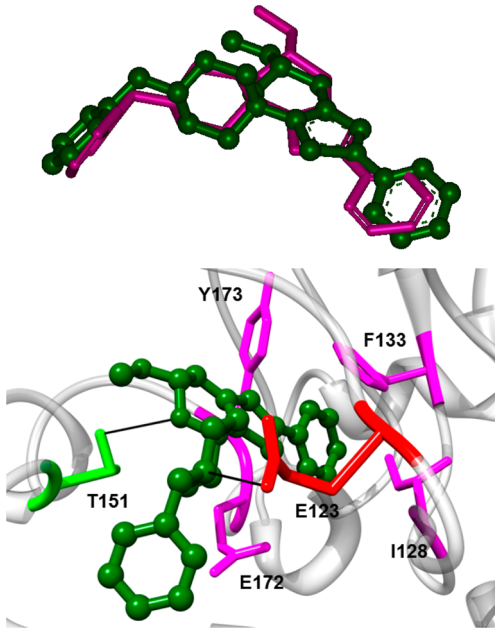

Figure 8. (Top) Comparison between the best conformation assumed by compound **6a** upon mapping the 3D pharmacophore model (purple sticks) and after docking in the putative σ_1 binding site (green sticks and balls). (Bottom) Equilibrated MD snapshots of the σ_1 receptor in complex with **6a**. The image is a zoomed view of the receptor binding site. The ligand is portrayed in green sticks and balls, while the protein residues mainly involved in the interaction with **6a** are highlighted as colored sticks and labeled. Salt bridge and H-bond interactions are shown as black lines. Water, ions, and counterions are not shown for clarity.

similarity between the molecular conformation adopted by the compound in mapping the 3D pharmacophore model and that assumed by the same compound in the σ_1 pocket upon binding. Most importantly, however, the best binding mode detected for **3h** after docking satisfies all ligand/protein intermolecular interactions required by pharmacophore hypothesis Hypo1. In detail, (i) the piperidinic nitrogen is engaged in a salt bridge with Asp126 (PI feature), (ii) the pyran oxygen atom H-bonds with the −NH group of the backbone peptidic linkage between Thr151 and Val152 (HBA feature), (iii) the aryl group linked to the thiophene ring is involved in stabilizing interactions with the aromatic components of Trp121 and Tyr120 (HYAr feature), and (iv) a network of hydrophobic interactions stabilizes the position of the thiophene and the *N*-benzylic rings among the residues Tyr173, Ile128, and Phe133 (two HY features).

Considering compound **6a** as a representative example of the derivatives featuring the phenyl ring in the left position, from the top panel of Figure 8 we can appreciate that, also in this case, the best molecular conformation mapping the 3D pharmacophore Hypo1 and the best binding mode of **6a** into the σ_1 binding pocket are superimposable. Quite surprisingly, however, the detailed inspection of the binding pose of **6a** reveals that, to comply with the pharmacophoric requirements upon protein binding, this molecule must adopt a "reverse" orientation with respect to that assumed by, e.g., **3h**, as shown in the bottom panel of Figure 8. Accordingly, the basic nitrogen of **6a** creates a salt bridge with Glu123 (PI feature), the oxygen atom of the pyran ring is engaged in a H-bond with the side chain −OH group of Thr131 (HBA feature), and the thiophene ring is stabilized by hydrophobic interactions with the side chains of both Tyr173 and E172 (HY feature). Notably, at variance with **3h**, the remaining hydrophobic pharmacophore requirement is fulfilled by the thiophene-linked phenyl ring, which aptly fits a small hydrophobic cavity lined by the side chains of Ile128 and Phe133.

All 40 receptor/drug complexes obtained from the pharmacophore-based docking procedure were then relaxed by energy minimization and molecular dynamics (MD) simulations, and finally, the relevant values of the free energy of binding, ΔG_{bind}, between all compounds and the σ_1 receptor were evaluated by applying the well-known MM/PBSA computational ansatz,[55,56] as listed in Table 9.

A plot of the ΔG_{bind} values calculated from simulations vs those obtained experimentally using the corresponding $K_i(\sigma_1)$ ($\Delta G_{bind(exptl)}$, last column in Table 9) shows a very good correlation coefficient (R^2 = 0.81; see Figure 9). Although this might be a somewhat expected result, given the structural similarity of the compounds considered, it is interesting to observe how MM/PBSA is able not only to rank all molecules in the correct order with respect to their affinity toward the σ_1 receptor but also to discriminate between high-affinity (e.g., ΔG_{bind} values ranging from approximately −12 to >−13 kcal/mol), intermediate-affinity (−10.5 kcal/mol < ΔG_{bind} < −12 kcal/mol), and low-affinity (ΔG_{bind} < −10.5 kcal/mol) compounds. The most notable result, however, is the fact that these calculations do support the reverse binding mode of the molecules with the phenyl substituent in the left position with respect to those featuring the same group in the top position. In fact, if we consider the MD snapshot of the ligand **3h**/σ_1 receptor complex shown in Figure 10A, we can observe how the main interactions detected after docking are totally preserved along the MD trajectory: a permanent salt bridge (average dynamic distance (ADL) = 4.03 ± 0.12 Å) is

dx.doi.org/10.1021/jm300894h | *J. Med. Chem.* 2012, 55, 8047−8065

Table 9. Experimentally Determined ($\Delta G_{bind(exptl)}$) and Calculated (ΔG_{bind}) Free Energy of Ligand/σ_1 Receptor Complexes[a]

compd of this paper	compd of ref 22	aryl	X	ΔH (kcal/mol)	$-T\Delta S$ (kcal/mol)	ΔG_{bind} (kcal/mol)	$\Delta G_{bind(exptl)}$ (kcal/mol)
	2a		H	−36.66 (0.18)	23.56 (0.37)	−13.10 (0.41)	−12.91
	3a		$-OCH_3$	−36.90 (0.19)	23.67 (0.39)	−13.23 (0.43)	−13.18
	2b	C_6H_5	H	−37.40 (0.18)	25.76 (0.42)	−11.64 (0.45)	−11.39
	2e	p-$MeOC_6H_5$	H	−38.36 (0.21)	25.83 (0.39)	−12.53 (0.44)	−12.04
	2c	p-MeC_6H_5	H	−38.50 (0.19)	25.69 (0.38)	−12.81 (0.42)	−11.52
	2f	p-$NO_2C_6H_5$	H	−38.70 (0.20)	25.91 (0.38)	−12.79 (0.43)	−11.97
	2g	p-CNC_6H_5	H	−38.63 (0.20)	26.02 (0.40)	−12.61 (0.45)	−11.56
	2d	1-napthyl	H	−39.06 (0.17)	26.18 (0.41)	−12.88 (0.44)	−11.46
	3b	C_6H_5	$-OCH_3$	−38.52 (0.22)	25.81 (0.37)	−12.71 (0.43)	−12.28
	3e	p-$MeOC_6H_5$	$-OCH_3$	−38.71 (0.18)	25.77 (0.39)	−12.94 (0.43)	−11.82
	3c	p-MeC_6H_5	$-OCH_3$	−38.51 (0.20)	25.79 (0.39)	−12.72 (0.44)	−11.87
	3f	p-$NO_2C_6H_5$	$-OCH_3$	−38.58 (0.18)	25.99 (0.40)	−12.59 (0.45)	−12.28
	3g	p-AcC_6H_5	$-OCH_3$	−38.43 (0.17)	25.56 (0.40)	−12.87 (0.43)	−12.00
	3h	p-CNC_6H_5	$-OCH_3$	−39.11 (0.16)	25.82 (0.40)	−13.29 (0.42)	−13.10
	3j	p-$CF_3C_6H_5$	$-OCH_3$	−38.13 (0.19)	25.64 (0.41)	−12.49 (0.43)	−11.25
	3d	1-naphthyl	$-OCH_3$	−38.38 (0.20)	26.03 (0.37)	−12.35 (0.42)	−11.33
	3i	3-pyridyl	$-OCH_3$	−38.67 (0.21)	25.98 (0.36)	−12.69 (0.41)	−11.82
	3k	p-biphenyl	$-OCH_3$	−38.08 (0.20)	26.30 (0.38)	−11.78 (0.43)	−10.27
9			$-OCH_3$	−36.82 (0.20)	23.61 (0.37)	−13.21 (0.42)	−12.96
4a		C_6H_5	$-OCH_3$	−36.31 (0.18)	24.48 (0.39)	−11.83 (0.43)	−11.27
4b		p-$MeOC_6H_5$	$-OCH_3$	−34.83 (0.19)	24.82 (0.41)	−10.01 (0.43)	−9.49
4c		p-CNC_6H_5	$-OCH_3$	−34.78 (0.18)	24.79 (0.42)	−9.99 (0.44)	−9.62
4d		p-biphenyl	$-OCH_3$	−34.71 (0.22)	24.95 (0.36)	−9.76 (0.42)	−9.09
10			H	−36.61 (0.21)	23.60 (0.36)	−13.01 (0.41)	−12.28
11			$-OCH_3$	−36.78 (0.18)	23.71 (0.41)	−13.07 (0.44)	−11.90
5a		C_6H_5	H	−36.07 (0.19)	24.53 (0.39)	−11.54 (0.43)	−11.76
6a		C_6H_5	$-OCH_3$	−35.80 (0.19)	24.74 (0.39)	−11.06 (0.43)	−10.64
6b		p-$MeOC_6H_5$	$-OCH_3$	−35.62 (0.20)	24.68 (0.40)	−10.94 (0.45)	−9.90
6c		p-MeC_6H_5	$-OCH_3$	−35.78 (0.17)	24.61 (0.38)	−11.17 (0.41)	−10.29
6d		p-$NO_2C_6H_5$	$-OCH_3$	−35.61 (0.17)	24.59 (0.37)	−11.02 (0.40)	−10.64
6e		p-AcC_6H_5	$-OCH_3$	−35.50 (0.17)	24.67 (0.41)	−10.83 (0.42)	−9.87
6f		p-CNC_6H_5	$-OCH_3$	−35.67 (0.21)	24.71 (0.38)	−10.96 (0.43)	−10.51
6g		p-$CF_3C_6H_5$	$-OCH_3$	−35.49 (0.19)	24.70 (0.39)	−10.79 (0.43)	−10.05
6h		1-naphthyl	$-OCH_3$	−35.72 (0.21)	24.81 (0.40)	−10.91 (0.45)	−10.81
6i		p-biphenyl	$-OCH_3$	−35.13 (0.20)	24.98 (0.40)	−10.15 (0.45)	−9.11
6j		3-pyridyl	$-OCH_3$	−36.08 (0.22)	24.82 (0.36)	−11.26 (0.42)	−11.74
7a		C_6H_5	H	−38.46 (0.18)	25.73 (0.38)	−12.73 (0.42)	−12.00
8a		C_6H_5	$-OCH_3$	−38.49 (0.18)	25.81 (0.38)	−12.68 (0.42)	−11.28
8b		p-$MeOC_6H_5$	$-OCH_3$	−38.51 (0.21)	25.91 (0.38)	−12.60 (0.43)	−11.12
8c		p-MeC_6H_5	$-OCH_3$	−38.69 (0.20)	25.88 (0.41)	−12.81 (0.46)	−11.69

[a] $\Delta G_{bind} = \Delta H - T\Delta S$. ΔH = enthalpic component of ΔG_{bind}. $-T\Delta S$ = entropic component of ΔG_{bind}. $\Delta G_{bind(exptl)}$ was estimated from the corresponding available $K_i(\sigma_1)$ values using the following relationship: $\Delta G_{bind(exptl)} = -RT \ln(1/K_i(\sigma_1))$.

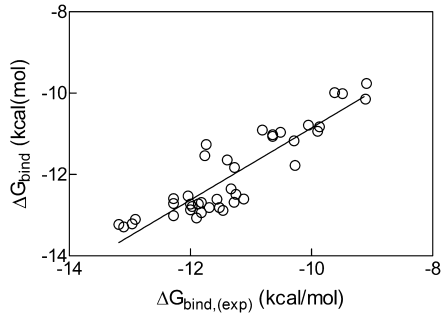

Figure 9. Correlation displaying the experimental vs estimated free energy of binding for all 40 ligand/σ_1 receptor complexes considered in this work.

established between the pyperidine NH^+ group and the $-COO^-$ moiety of Asp126, a persistent H-bond, characterized by an ADL of 1.93 ± 0.18 Å, is detected between the backbone NH group of Thr151 and Val152 and the O atom of the pyran ring of **3h**, a number of stabilizing $\pi-\pi$ interactions take place, involving the side chains of Trp121 and Tyr173 and the ligand benzonitrile and thiophene rings, respectively, and last, the *N*-benzyl group of **3h** remains nicely encased within the hydrophobic pocket generated by residues Ile128 and Phe133. These plethora of favorable, stabilizing interactions result in a calculated value of ΔG_{bind} of −13.29 kcal/mol, in excellent agreement with the corresponding experimental value (−13.10 kcal/mol; see Table 9), thereby confirming the ranking of **3h** as one of the most potent σ_1 ligands of the entire series.

In the case of compound **6a**, a template molecule representative of all derivatives bearing the phenyl ring in the left position, the protein/ligand interactions depicted at the end of the pharmacophore-assisted docking phase are again

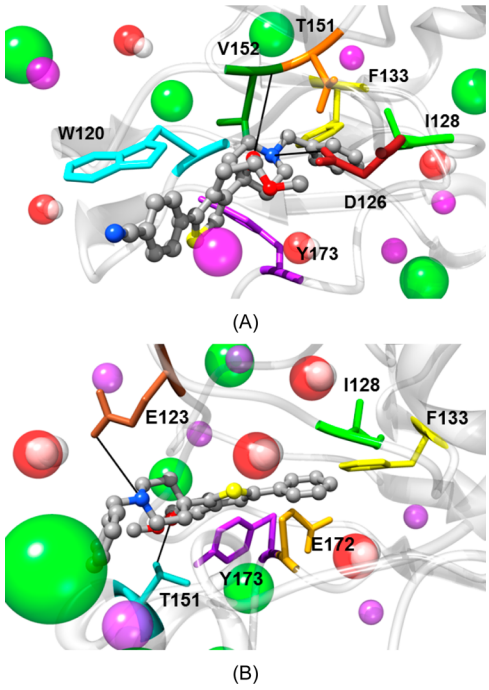

Figure 10. Equilibrated MD snapshots of **3h** (A) and **6a** (B) in complex with the σ_1 receptor. The images are zoomed views of the receptor binding site. The protein structure is depicted as a transparent gray ribbon, while both ligands are shown in atom-colored sticks and balls (C, gray; O, red; S, yellow; N, blue; H atoms are omitted). The protein residues mainly involved in the interaction with the ligands are highlighted as colored sticks and labeled. Salt bridge and H-bond interactions are shown as black lines. Some water molecules, ions, and counterions are displayed as atom-colored spheres (O, red; H, white; Na^+, purple; Cl^-, green).

detected and preserved during the entire MD simulation. In detail, a stable H-bond (ADL = 1.88 ± 0.15 Å) is found between the side chain −OH group of Thr181 and the pyran ring oxygen of **6a**, while a salt bridge (ADL = 3.98 ± 0.22 Å) between the CO_2^- group of Glu123 and the piperidine NH^+ of **6a** is also evidence for the whole simulation period. Favorable hydrophobic interactions are generated between the phenyl substituent and the side chains of Ile128 and Phe133, and last, the thiophene moiety of **6a** is engaged in a positive $\pi-\pi$ interaction with the aromatic side chain of Tyr173 and is further stabilized by the influence of the vicinal alkyl chain of Glu172.

5. CONCLUSION

The introduction of aryl moieties in the α- and β-positions of complex spirocyclic σ_1 ligands was performed by regioselective direct C−H bond arylation using the catalyst systems $PdCl_2$/2,2′-bipyridyl/Ag_2CO_3 and $PdCl_2$/$P[OCH(CF_3)_2]_3$/Ag_2CO_3, respectively. This late-stage functionalization allows the synthesis of a large library of diversely substituted spirocyclic σ_1 ligands, which represent the basis for the development of a pharmacophore model. The main features of the pharmacophore are a positive ionizable group, a hydrogen bond acceptor group, two hydrophobic moieties, and one hydrophobic aromatic point. Validation using test set compounds confirms the high quality of the pharmacophore model. The interactions of the spirocyclic σ_1 ligands with the receptor protein were analyzed by docking into a 3D homology model of the σ_1 receptor. These docking experiments led to a very good correlation between the experimentally determined free energy of the ligand binding (calculated from the K_i value) and the estimated free energy from the model. The most striking result of these calculations is the reverse binding mode of ligands with the phenyl moiety in the top position compared with ligands bearing the aryl moiety in the left position. Moreover, the contribution of single amino acid residues to the overall binding of both types of ligands was analyzed using the docking experiments.

6. EXPERIMENTAL SECTION

Chemistry. *General Procedures.* Silica gel 60 F254 plates (Merck) were used for thin-layer chromatography (TLC). ^1H NMR (400, 300, and 600 MHz) and ^{13}C NMR (100 MHz) spectra were recorded on a Unity Mercury Plus 400 (400 MHz) NMR spectrometer (Varian), a JNM-ECA-400 (400 MHz) spectrometer (JEOL), a Bruker AV 300 (300 MHz) spectrometer, and a Varian Unity Plus 600 (600 MHz) spectrometer operating at 23 °C; chemical shifts δ are reported in parts per million (ppm) against the reference compound tetramethylsilane and calculated using the chemical shift of the signal of the residual nondeuterated solvent. Finnigan MAT 4200s, Bruker Daltonics Micro Tof, and Waters Micromass Quatro LCZ spectrometers were used for HRMS (ESI); peaks are given in m/z (percentage of the base peak). The purity of all test compounds was greater than 95%, which was determined by HPLC method A or B (see the Supporting Information).

General Procedure A for the α-Arylation of Spirocyclic Thiophenes with Iodoarenes. A 20 mL glass vessel was equipped with a magnetic stirring bar and closed by a J. Young O-ring tap. The flask was flame-dried under vacuum and filled with Ar after being cooled to rt. Under a permanent stream of Ar, the catalyst $PdCl_2$/bipy (10 mol %) and Ag_2CO_3 (1 equiv) were filled into the vessel and suspended in dry *m*-xylene (0.4 mL). This mixture was stirred at 60 °C for 30 min. Finally, a solution of the iodoarene (1.1 equiv) and a solution of the spirocyclic starting material (1 equiv) in dry *m*-xylene (0.6 mL in total) were added dropwise. The vessel was sealed with the O-ring tap and heated at 150 °C for 12 h in an eight-well reaction block. After the vessel was cooled to rt, the mixture was filtered through a short silica pad (EtOAc). The filtrate was concentrated in vacuo, and the crude product was purified by gel permeation chromatography ($CHCl_3$) followed by preparative thin-layer chromatography or flash chromatography (short column) to yield the corresponding arylthiophene in high purity.

General Procedure B for the β-Arylation of Spirocyclic Thiophenes with Iodoarenes. A 20 mL glass vessel was equipped with a magnetic stirring bar and closed by a J. Young O-ring tap. The flask was flame-dried under vacuum and filled with Ar after being cooled to rt. Under a permanent stream of Ar, $PdCl_2$ (10 mol %) and Ag_2CO_3 (1 equiv) were filled into the vessel. The phosphite ligand $P[OCH(CF_3)_2]_3$ (20 mol %) and subsequently dry *m*-xylene (0.5 mL) were added, and this mixture was stirred at 60 °C for 30 min to form the active catalyst. Finally, a solution of the iodoarene (1.1 equiv) and a solution of the spirocyclic starting material (1 equiv) in dry *m*-xylene (0.5 mL in total) were added. The vessel was sealed with the O-ring tap and heated at 150 °C for 12 h in an eight-well reaction block. After the vessel was cooled to rt, the mixture was filtered through a short silica pad (EtOAc). The filtrate was concentrated in vacuo, and the crude product was purified by gel permeation chromatography ($CHCl_3$) followed by preparative thin-layer chromatography or flash chromatography (short column) to yield the corresponding arylthiophene in high purity.

*1-Benzyl-6′-methoxy-2′-phenyl-6′,7′-dihydrospiro[piperidine-4,4′-thieno[3,2-c]pyran] (**4a**).* According to general procedure A, the spirocyclic thiophene **9** (33.2 mg, 0.101 mmol) was reacted with iodobenzene (12.4 μL, 0.11 mmol), Ag_2CO_3 (27.5 mg, 0.01 mmol), and $PdCl_2$/bipy (3.2 mg, 0.01 mmol) in *m*-xylene (1.2 mL). The crude product was purified by $CHCl_3$ GPC and FC (1.5 cm, h = 5 cm, hexane:EtOAc = 4:1, 3 mL, R_f = 0.10): colorless solid; mp 137 °C; yield 23.4 mg (57%) after GPC; yield 18.9 mg (46%) after FC; ^1H

dx.doi.org/10.1021/jm300894h | J. Med. Chem. 2012, 55, 8047−8065

NMR ($CDCl_3$) δ (ppm) = 1.84−2.01 (m, 3H, $N(CH_2CH_2)_2$), 2.15 (td, J = 13.2/4.4 Hz, 1H, $N(CH_2CH_2)_2$), 2.45 (td, J = 11.6/3.3 Hz, 1H, $N(CH_2CH_2)_2$), 2.54 (td, J = 12.4/2.5 Hz, 1H, $N(CH_2CH_2)_2$), 2.74−2.81 (m, 2H, $N(CH_2CH_2)_2$), 2.86 (dd, J = 15.8/7.2 Hz, 1H, thioph CH_2CH), 2.99 (dd, J = 15.8/3.3 Hz, 1H, thioph CH_2CH), 3.57 (s, 3H, OCH_3), 3.57 (d, J = 13.0 Hz, 1H, NCH_2Ph), 3.61 (d, J = 13.1 Hz, 1H, NCH_2Ph), 4.91 (dd, J = 7.2/3.3 Hz, 1H, thioph CH_2CH), 7.02 (s, 1H, 3′-*H*-thioph), 7.27−7.41 (m, 8H, Ph *H*), 7.49 − 7.54 (m, 2H, Ph *H*).

*1-Benzyl-2′-phenyl-4′,5′-dihydrospiro[piperidine-4,7′-thieno[2,3-c]pyran] (**5a**)*. According to general procedure A, the spirocyclic thiophene **10** (29.4 mg, 0.098 mmol) was reacted with iodobenzene (12.1 μL, 0.11 mmol), Ag_2CO_3 (29.2 mg, 0.11 mmol), and $PdCl_2$/bipy (3.4 mg, 0.01 mmol) in *m*-xylene (1.2 mL). The crude product was purified by $CHCl_3$ GPC and FC (1.5 cm, h = 5 cm, hexane:EtOAc = 3:2, 3 mL, R_f = 0.52): colorless resin; yield 23.6 mg (64%) after GPC; yield 14.5 mg (40%) after FC; ^{1}H NMR ($CDCl_3$) δ (ppm) = 1.94−2.09 (m, 4H, $N(CH_2CH_2)_2$), 2.43 (td, J = 11.3/4.1 Hz, 2H, $N(CH_2CH_2)_2$), 2.69 (t, J = 5.5 Hz, 2H, thioph CH_2CH_2), 2.74 (d, J = 11.6 Hz, 2H, $N(CH_2CH_2)_2$), 3.57 (s, 2H, NCH_2Ph), 3.94 (t, J = 5.5 Hz, 2H, thioph CH_2CH_2), 6.96 (s, 1H, 3′-*H*-thioph), 7.22−7.25 (m, 1H, Ph *H*), 7.27−7.29 (m, 1H, Ph *H*), 7.29−7.41 (m, 6H, Ph *H*), 7.51−7.56 (m, 2H, Ph *H*).

*1-Benzyl-5′-methoxy-2′-phenyl-4′,5′-dihydrospiro[piperidine-4,7′-thieno[2,3-c]pyran] (**6a**)*. According to general procedure A, the spirocyclic thiophene **11** (19.5 mg, 0.060 mmol) was reacted with iodobenzene (7.5 μL, 0.07 mmol), Ag_2CO_3 (17.3 mg, 0.06 mmol), and $PdCl_2$/bipy (2.1 mg, 0.006 mmol) in *m*-xylene (1.0 mL). The crude product was purified by $CHCl_3$ GPC and preparative TLC (h = 15 cm, hexane:EtOAc = 3:2, R_f = 0.5): colorless solid; yield 9.2 mg (38%) after $CHCl_3$ GPC; yield 4.5 mg (19%) after preparative TLC; ^{1}H NMR ($CDCl_3$) δ (ppm) = 1.91−2.07 (m, 2H, $N(CH_2CH_2)_2$), 2.08−2.17 (m, 2H, $N(CH_2CH_2)_2$), 2.47 (td, J = 11.5/2.8 Hz, 1H, $N(CH_2CH_2)_2$), 2.57 (td, J = 11.8/2.9 Hz, 1H, $N(CH_2CH_2)_2$), 2.72 (dd, J = 15.5/7.4 Hz, 1H, thioph CH_2CH), 2.77−2.84 (m, 2H, $N(CH_2CH_2)_2$), 2.87 (dd, J = 15.5/3.3 Hz, 1H, thioph CH_2CH), 3.57 (s, 3H, OCH_3), 3.57 (d, J = 13.2 Hz, 1H, NCH_2Ph), 3.61 (d, J = 13.2 Hz, 1H, NCH_2Ph), 4.92 (dd, J = 7.3/3.3 Hz, 1H, thioph CH_2CH), 6.94 (s, 1H, 3′-*H*-thioph), 7.27−7.39 (m, 8H, Ph *H*), 7.49−7.54 (m, 2H, Ph *H*).

*1-Benzyl-3′-phenyl-4′,5′-dihydrospiro[piperidine-4,7′-thieno[2,3-c]pyran] (**7a**)*. According to general procedure B, the spirocyclic thiophene **10** (31.3 mg, 0.105 mmol) was reacted with iodobenzene (12.8 μL, 0.11 mmol), Ag_2CO_3 (28.1 mg, 0.10 mmol), $PdCl_2$ (2.0 mg, 0.01 mmol), and $P[OCH(CF_3)_2]_3$ (7.1 μL, 0.02 mmol) in *m*-xylene (1.2 mL). The crude product was purified by $CHCl_3$ GPC and preparative TLC (h = 15 cm, hexane:EtOAc = 10:1, R_f = 0.06, four runs): pale yellow resin; yield 8.2 mg (21%) (mixture of regioisomers) after GPC; yield 2.5 mg (6%) after preparative TLC; ^{1}H NMR ($CDCl_3$) δ (ppm) = 1.96−2.08 (m, 4H, $N(CH_2CH_2)_2$), 2.44 (td, J = 11.4/4.0 Hz, 2H, $N(CH_2CH_2)_2$), 2.69 (t, J = 5.4 Hz, 2H, thioph CH_2CH_2), 2.75 (d, J = 11.5 Hz, 2H, $N(CH_2CH_2)_2$), 3.57 (s, 2H, NCH_2Ph), 3.90 (t, J = 5.4 Hz, 2H, thioph CH_2CH_2), 7.13 (s, 1H, 2′-*H*-thioph), 7.27−7.42 (m, 10H, Ph *H*).

*1-Benzyl-5′-methoxy-3′-phenyl-4′,5′-dihydrospiro[piperidine-4,7′-thieno[2,3-c]pyran] (**8a**)*. According to general procedure B, the spirocyclic thiophene **11** (48 mg, 0.15 mmol) was reacted with iodobenzene (17.9 μL, 0.16 mmol), Ag_2CO_3 (46.6 mg, 0.17 mmol), $PdCl_2$ (2.9 mg, 0.016 mmol), and $P[OCH(CF_3)_2]_3$ (10.3 μL, 0.032 mmol) in *m*-xylene (1.5 mL). The crude product was purified by $CHCl_3$ GPC and preparative TLC (h = 15 cm, hexane:EtOAc = 14:1, 2% NEt_3, R_f = 0.1, seven runs): colorless solid; yield 18.9 mg (32%) (mixture of regioisomers) after GPC; yield 7.5 mg (13%) after preparative TLC; ^{1}H NMR ($CDCl_3$) δ (ppm) = 1.97 (td, J = 12.8/3.3 Hz, 1H, $N(CH_2CH_2)_2$), 2.02−2.16 (m, 3H, $N(CH_2CH_2)_2$), 2.49 (td, J = 12.1/2.4 Hz, 1H, $N(CH_2CH_2)_2$), 2.59 (td, J = 11.6/2.9 Hz, 1H, $N(CH_2CH_2)_2$), 2.74−2.86 (m, 4H, $N(CH_2CH_2)_2$, thioph CH_2CH), 3.54 (s, 3H, OCH_3), 3.58 (d, J = 13.7 Hz, 1H, NCH_2Ph), 3.61 (d, J = 13.4 Hz, 1H, NCH_2Ph), 4.85 (dd, J = 6.8/3.7 Hz, 1H, thioph CH_2CH), 7.16 (s, 1H, 2′-*H*-thioph), 7.27−7.41 (m, 10H, Ph *H*).

*1-Benzyl-4′,5′-dihydrospiro[piperidine-4,7′-thieno[2,3-c]pyran] (**10**)*. The enol ether **16** (106.8 mg, 0.36 mmol) was dissolved in dry MeOH (10 mL), and 10% Pd/C (11 mg) was added. The suspension was stirred under a H_2 atmosphere (balloon) at rt for 18 h. Afterward the catalyst was filtered off, and the remaining residue was washed first with 2 M HCl and then with water. The filtrate was alkalized with 2 M NaOH and extracted twice with CH_2Cl_2. The organic layers were separated, combined, and dried over K_2CO_3. The solvent was removed in vacuo, and the crude product was purified by FC (3.5 cm, h = 15 cm, cyclohexane:EtOAc = 9:1, 2% NEt_3, 10 mL, R_f = 0.27): colorless solid; mp 65 °C; yield 72 mg (67%); ^{1}H NMR ($CDCl_3$) δ (ppm) = 1.90−2.05 (m, 4H, $N(CH_2CH_2)_2$), 2.37−2.50 (m, 2H, $N(CH_2CH_2)_2$), 2.69 (t, 5.5 Hz, 2H, thioph CH_2CH_2), 2.72−2.80 (m, 2H, $N(CH_2CH_2)_2$), 3.58 (s, 2H, NCH_2Ph), 3.91 (t, J = 5.5 Hz, 2H, thioph CH_2CH_2), 6.76 (d, 5.0 Hz, 1H, 3′-*H*-thioph), 7.13 (d, 5.0 Hz, 1H, 2′-*H*-thioph), 7.27−7.38 (m, 5H, Ph *H*).

*1-Benzyl-5′-methoxy-4′,5′-dihydrospiro[piperidine-4,7′-thieno-[2,3-c]pyran] (**11**)*. The hydroxy acetal **13** (2.1 g, 5.81 mmol) was dissolved in dry MeOH (50 mL), and *p*-toluenesulfonic acid (1.25 g, 7.24 mmol) was added. The solution was stirred for 24 h at rt. Then 2 M NaOH was added until pH 8, and the solution was diluted with water (50 mL). The aqueous layer was extracted twice with CH_2Cl_2. The combined organic layers were dried (K_2CO_3) and filtered, and the solvent was removed in vacuo. The remaining oil was purified by FC (6 cm, h = 15 cm, cyclohexane:EtOAc = 4:1, 30 mL, R_f = 0.30): colorless solid; mp 77 °C; yield 1.04 g (54%); ^{1}H NMR ($CDCl_3$) δ (ppm) = 1.87−2.02 (m, 2H, $N(CH_2CH_2)_2$), 2.10 (td, J = 13.7/4.4 Hz, 2H, $N(CH_2CH_2)_2$), 2.47 (td, J = 12.1/2.7 Hz, 1H, $N(CH_2CH_2)_2$), 2.57 (td, J = 11.8/3.1 Hz, 1H, $N(CH_2CH_2)_2$), 2.66−2.82 (m, 3H, thioph CH_2CH, $N(CH_2CH_2)_2$), 2.88 (dd, J = 15.5/3.3 Hz, 1H, thioph CH_2CH), 3.56 (d, J = 13.1 Hz, 1H, NCH_2Ph), 3.57 (s, 3H, OCH_3), 3.61 (d, J = 13.1 Hz, 1H, NCH_2Ph), 4.89 (dd, J = 7.4/3.3 Hz, 1H, thioph CH_2CH), 6.74 (d, J = 5.0 Hz, 1H, 3′-*H*-thioph), 7.16 (d, J = 5.0 Hz, 1H, 2′-*H*-thioph), 7.27−7.41 (m, 5H, Ph *H*).

Receptor Binding Studies. The σ_1 and σ_2 receptor affinities were recorded according to refs 39−42 The procedures are given in detail in the Supporting Information.

Molecular Modeling. *Pharmacophore Modeling.* The model structures of all compounds were built using the 2D−3D sketcher of Discovery Studio Catalyst (DS, version 2.5, Accelrys, San Diego, CA). High-quality conformational models are crucial for the development of predictive pharmacophore models. Accordingly, in this study we employed an ad hoc procedure to derive molecular conformations, instead of using those automatically generated by DS Catalyst, for a better quality in covering the low-energy conformational space.[51] Each molecular structure was subjected to energy minimization using the generalized CHARMM force field[57] until the gradient dropped below 0.05. The minimized structures were used as the starting point for subsequent conformational searches. A 10000-step Monte Carlo torsional sampling conformational search was conducted for each compound. Unique low-energy conformations within 20 kcal/mol of the corresponding global energy minimum were collected for each molecule. A conformation was considered unique only when the maximum displacement of at least one heavy atom was greater than 0.5 Å. A maximum of 250 unique conformations were recovered for each compound. The classical conformational search was also carried out using the Poling algorithm[58] and the CHARMM force field as implemented in the DS Catalyst program for comparison. The "best quality" generation option was adopted to select representative conformers over a 0−20 kcal/mol interval above the computed global energy minimum in the conformational space, and again the number of conformers generated for each compound was limited to a maximum of 250. Comparing the results of the two conformational searches, we verified the existence of considerable differences between the two approaches in generating conformations for saturated six-membered rings such as piperidine. This group is quite common in drug molecules and constitutes a popular molecular scaffold. A survey of the crystal structures of druglike molecules and protein/ligand complexes available in the literature and in public databases reveals that this saturated ring overwhelmingly adopts low-energy chair

conformations. The conformational search conducted with the typical DS Catalyst settings described above, however, generated predominantly twisted conformations which might lead to an incorrect mapping of this functionally important group. In comparison, the alternative procedure of conformational search produced a considerable number of chair conformations for this heterocyclic moiety. The main drawback of this technique, however, is that it takes considerably longer to generate the relevant conformational models. Nonetheless, as the spirit of the work was the generation of a predictive 3D pharmacophore model for these classes of compounds, we considered it worthwhile to use more accurate conformational models.

On the basis of the conformations for each compound, the DS Catalyst Hypothesis module was used to generate three-dimensional pharmacophore models. During hypothesis generation, the software attempts to minimize a cost function containing two main terms: the first penalizes the deviation between the estimated affinities of the training set molecules and their experimental values, while the second penalizes the complexity of the hypothesis. The uncertainty factor for each compound represents the ratio range of uncertainty in the affinity value based on the expected statistical irregularity of biological data collection. Uncertainty influences the first step—also called the constructive phase—of the hypothesis-generating process. In this work, an uncertainty of 1.1 was preferred over the default factor of 3.0, as the experimental affinities of our compounds barely span the required 4 orders of magnitude.

An analysis of the functional groups characterizing our compounds suggested that HYAr, aliphatic (HYAl) and generic HY, HBA, and PI features could effectively map the critical chemical features and, hence, describe the σ_1 receptor affinity of our compounds. Accordingly, these five features were selected to constitute the essential information in the automated hypothesis generation process.

Three validation procedures were used to determine the statistical relevance and the validity of the proposed 3D pharmacophore models: the test set prediction method, the CatScramble method, and the leave-one-out procedure. In this work, the first procedure consisted of the collection of further, different compounds into a test set and performing a regression analysis by mapping the test set molecules onto the best pharmacophore hypothesis. The high correlation coefficients obtained using the test set compounds revealed the good correlation between the actual and estimated affinities and, hence, the predictive validity of the corresponding 3D hypothesis. The CatScramble validation procedure is based on Fisher's randomization test.[59] The goal of this type of validation is to check whether there is a strong correlation between the chemical structures and the binding affinity. This is done by randomizing the affinity data associated with the training set compounds, generating pharmacophore hypotheses using the same features and parameters employed to develop the original pharmacophore model. The statistical significance is calculated according to the following formula:

$$\text{significance} = 100[1 - (1 + x/y)]$$

where x is the total number of hypotheses having a total cost lower than that of the original (best) hypothesis and y is the total number of DS Catalyst Hypothesis runs (initial + random runs). Thus, 49 random spreadsheets (i.e., 49 DS Catalyst Hypothesis runs) have to be generated to obtain a 98% confidence level. Should any randomized data set result in the generation of a 3D pharmacophore with similar or even better cost values, root-mean-square deviations, and correlation coefficients, then it is likely that the original hypothesis does reflect a chance correlation.

Finally, the leave-one-out test checks if the correlation between experimental and computed affinities is heavily dependent on one particular molecule of the training set by recomputing the pharmacophore model with the exclusion of one molecule at a time. Accordingly, 27 new training sets were derived, each composed of 30 molecules, and 27 DS Catalyst Hypothesis calculations were performed under the same conditions. For each run, the hypothesis characterized by the lowest total cost was employed to predict the affinity of the excluded compound and to estimate the new correlation coefficient.

Receptor Docking and MM/PBSA Scoring. The model structures of the selected ligands were generated with DS. All molecules were subjected to an initial energy minimization, with the convergence criterion set to 10^{-4} kcal/(mol Å). A conformational search was carried out using a well-validated, ad hoc developed combined molecular mechanics/molecular dynamics simulated annealing (MDSA) protocol[60] using Amber 11.[61] Accordingly, the relaxed structures were subjected to five repeated temperature cycles (from 310 to 1000 K and back) using constant-volume/constant-temperature (NVT) MD conditions. At the end of each annealing cycle, the structures were again energy minimized to converge below 10^{-4} kcal/(mol Å), and only the structures corresponding to the minimum energy were used for further modeling. The atomic partial charges for the geometrically optimized compounds were obtained using the RESP procedure,[62] and the electrostatic potentials were produced by single-point quantum mechanical calculations at the Hartree−Fock level with a 6-31G* basis set, using the Merz−Singh−Kollman van der Waals parameters.[63,64] Eventual ff03[65] missing force field parameters for the inhibitor molecules were generated using the general Amber force field (GAFF)[66] of Amber 11.

The optimized structures of all compounds were then docked into the σ_1 putative binding pockets by applying a consolidated procedure;[50,56,60] accordingly, it will be described here only briefly. All docking experiments were performed with Autodock 4.3/Autodock Tools 1.4.6[67] on a win64 platform. DS was employed to define the size of the binding site, using an opening site of 10 Å and a grid size of 0.7 Å. The dimensions of the Autodock grid box, based on the cavity identified by DS, was large enough to cover all possible rotations of each ligand. van der Waals interactions and hydrogen bonding (O−H, N−H, and S−H) were modeled with the Amber 12-6 and 12-10 Lennard-Jones parameters, respectively, while the distance-dependent relative permittivity of Mehler and Solmajer[68] was applied in the generation of the electrostatic grid maps. A total of 300 Monte Carlo/simulated annealing (MC/SA) runs were performed, with 100 constant-temperature cycles for simulated annealing. The GB/SA implicit water model[69] was used in these calculations to mimic the solvated environment. The angles of the side chains and the rotation of the angles φ and ψ were set free during the calculations, while all others parameters of the MC/SA algorithm were kept as default. The structures of all compounds were subjected to cluster analysis with a 1 Å tolerance for an all-atom root-mean-square (rms) deviation from a lower energy structure representing each cluster family. The resulting docked conformations were clustered and visualized; then, for each compound, only the molecular conformation satisfying the combined criteria of (i) having the lowest (i.e., more favorable) Autodock energy, (ii) belonging to a highly populated cluster, and (iii) satisfying the specific 3D pharmacophore requirements was selected to carry for further modeling.

Each ligand/receptor complex obtained from the docking procedure was further refined in Amber 11[61] using the quenched molecular dynamics (QMD) method.[50,56,60] According to QMD, 1 ns MD simulations at 300 K were employed to sample the conformational space of each ligand/receptor complex in the GB/SA continuum solvation environment.[69] The integration step was equal to 1 fs. After each picosecond, each system was cooled to 0 K, and the structure was extensively minimized and stored. To prevent global conformational changes of the protein, the backbone atoms of the protein binding site were constrained by a harmonic force constant of 100 kcal/Å, whereas the amino acid side chains and the ligands were allowed to move without any constraint. The best energy configuration of each complex resulting from the previous step was subsequently solvated by a cubic box of TIP3P[70] water molecules extending at least 10 Å in each direction from the solute. The system was then neutralized with the addition of 21 Na^+ and 15 Cl^- counterions; furthermore, the solution ionic strength was adjusted to the physiological value of 0.15 M by adding the required amounts of Na^+ and Cl^- ions.

Each solvated system was relaxed by 500 steps of steepest descent followed by 500 other conjugate-gradient minimization steps and then gradually heated to a temperature of 300 K in intervals of 50 ps of NVT MD, using a Verlet integration time step of 1.0 fs. The Langevin

thermostat was used to control temperature, with a collision frequency of 2.0 ps^{-1}. The SHAKE method[71] was used to constrain all of the covalently bound hydrogen atoms, while long-range nonbonded van der Waals interactions were truncated by using dual cutoffs of 6 and 12 Å. The particle mesh Ewald (PME) method[72] was applied to treat long-range electrostatic interactions. The protein was restrained with a force constant of 2.0 kcal/(mol Å), and all simulations were carried out with periodic boundary conditions.

The density of each system was subsequently equilibrated via MD runs in the isothermal−isobaric (NPT) ensemble, with isotropic position scaling and a pressure relaxation time of 1.0 ps, for 50 ps with a time step of 1 fs. All restraints on the protein atoms were then removed, and each system was further equilibrated using NPT MD runs at 300 K, with a pressure relaxation time of 2.0 ps. Three equilibration steps were performed, each 2 ns long and with a time step of 2.0 fs. To check the system stability, the fluctuations of the rmsd of the simulated position of the backbone atoms of the σ_1 receptor with respect to those of the initial protein were monitored. All chemicophysical parameters and rmsd values showed very low fluctuations at the end of the equilibration process, indicating that the systems reached a true equilibrium condition.

Each equilibration phase was followed by a data production run consisting of 4 ns of MD simulations in the canonical (constant volume−constant temperature, NVT) ensemble. Only the last 2 ns of each equilibrated MD trajectory weas considered for statistical data collections. A total of 100 trajectory snapshots were analyzed for each drug/receptor complex.

The binding free energy, ΔG_{bind}, between each ligand and the σ_1 receptor was estimated by resorting to the MM/PBSA approach.[55] According to this well-validated methodology,[50,56,60,73] the binding free energy between two biological entities (e.g., a drug and its protein target) in a solvent was obtained as the sum of the interaction energy between the receptor and the ligand (ΔE_{MM}), the solvation free energy (ΔG_{sol}), and the conformational entropy contribution ($-T\Delta S$), averaged over a series of snapshots from the corresponding MD trajectories:

$$\Delta G_{bind} = \Delta E_{MM} + \Delta G_{solv} - T\Delta S \quad (1)$$

The ΔE_{MM} term in eq 1 can be obtained directly from the molecular mechanics interaction energies as

$$\Delta E_{MM} = \Delta E_{int} + \Delta E_{vdW} + \Delta E_{ele} \quad (2)$$

where ΔE_{int}, ΔE_{vdW}, and ΔE_{ele} are the internal, van der Waals, and electrostatic components of the nonbonded interaction energy, respectively. Since in this work we adopted the "single trajectory protocol", $\Delta E_{int} = 0$ in eq 2.

The second term in eq 1, the solvation energy ΔG_{sol}, can also be partitioned into two different contributions:

$$\Delta G_{solv} = \Delta G_{PB} + \Delta G_{NP} \quad (3)$$

The polar term of ΔG_{solv}, ΔG_{PB}, was estimated using DelPhi,[74] which solves the Poisson−Boltzmann equations numerically and calculates the electrostatic energy according to the electrostatic potential. In these calculations, the interior and exterior dielectric constant values were set equal to 1 and 80, respectively. A grid spacing of 0.5 per angstrom, extending 20% beyond the dimensions of the solute, was employed. The value of the nonpolar component of ΔG_{solv}, ΔG_{NP}, was calculated using the following relationship:[75]

$$\Delta G_{NP} = \gamma(SA) + \beta \quad (4)$$

in which γ = 0.00542 kcal/(mol $Å^2$), β = 0.92 kcal/mol, and SA is the molecular surface area estimated by means of the MSMS software.[76]

The change in solute entropy upon association ($-T\Delta S$ in eq 1) was evaluated using the Nmode module of Amber 11.[61] The normal-mode analysis[77] was performed for the minimized structures of the complexes, σ_1 receptor, and ligands using a distance-dependent dielectric constant $\varepsilon = 4r_{ij}$. In the first step of this calculation, an 8 Å sphere around the ligand was cut out from an MD snapshot for each ligand/protein complex. This value was shown to be large enough to yield converged mean changes in solute entropy. On the basis of the size-reduced snapshots of the complex, we generated structures of the uncomplexed reactants by removing the atoms of the protein and ligand. Each of those structures was minimized, using a distance-dependent dielectric constant $\varepsilon = 4r$, to account for solvent screening, and its entropy was calculated using classical statistical formulas and normal-mode analysis. To minimize the effects due to different conformations adopted by individual snapshots, we averaged the estimation of entropy over 40 snapshots.

The entire MD simulation and data analysis procedure was optimized by integrating Amber 11 in modeFRONTIER, a multidisciplinary and multiobjective optimization and design environment.[78]

■ ASSOCIATED CONTENT

Ⓢ Supporting Information

Physical and spectroscopic data of all new compounds, purity data, general chemistry methods, and details of the receptor binding studies. This material is available free of charge via the Internet at http://pubs.acs.org.

■ AUTHOR INFORMATION

Corresponding Author

*Phone/fax: +81-52-788-6098 (K.I.). Phone: +39-040-5583750 (S.P.); +49-251-8333311 (B.W.). Fax: +39-040-569823 (S.P.); +49-251-8332144 (B.W.). E-mail: itami.kenichiro@a.mbox.nagoya-u.ac.jp (K.I.); sabrina.pricl@di3.units.it (S.P.); wuensch@uni-muenster.de (B.W.).

Notes

The authors declare no competing financial interest.

■ ACKNOWLEDGMENTS

This work was performed within the framework of the International Research Training Group (IRTG) "Complex Functional Systems in Chemistry: Design, Synthesis and Applications" in collaboration with the University of Nagoya. Financial support of the IRTG and this project by the Deutsche Forschungsgemeinschaft is gratefully acknowledged. E.L., V.D.C., and S.P. acknowledge financial support from ESTECO through the project Drug Discovery and Optimization by Simulation (DDOS).

■ ABBREVIATIONS USED

MW, molecular weight; NMDA, *N*-methyl-D-aspartate; MM/PBSA, molecular mechanics/Poisson−Boltzmann surface area; rmsd, root-mean-square deviation; PI, positive ionizable; HBA, hydrogen bond acceptor; HY, hydrophobic moiety; HYAr, hydrophobic aromatic point; HYAl, hydrophobic aliphatic; MD, molecular dynamics; ADL, average dynamic length; THF, tetrahydrofuran

■ REFERENCES

(1) Falkenstein, E.; Meyer, C.; Eisen, C.; Scriba, P. C.; Wehling, M. Full-length cDNA sequence of a progesterone membrane-binding protein from porcine vascular smooth muscle cells. *Biochem. Biophys. Res. Commun.* **1996**, *229*, 86−89.

(2) Xu, J.; Zeng, C.; Chu, W.; Pan, F.; Rothfuss, J. M.; Zhang, F.; Tu, Z.; Zhou, D.; Zeng, D.; Vangveravong, S.; Johnston, F.; Spitzer, D.; Chang, K. C.; Hotchkiss, R. S.; Hawkins, W. G.; Wheeler, K. T.; Mach, R. H. Identification of the PGRMC1 protein complex as the putative sigma-2 receptor binding site. *Nat. Commun.* **2011**, *2*, No. 380.

(3) Hanner, M.; Moebius, F. F.; Flandorfer, A.; Knaus, H.-G.; Striessnig, J.; Kempner, E.; Glossmann, H. Purification, molecular cloning, and expression of the mammalian sigma$_1$-binding site. *Proc. Natl. Acad. Sci. U.S.A.* **1996**, *93*, 8072−8077.

(4) Seth, P.; Fei, Y.-J.; Li, H. W.; Huang, W.; Leibach, F. H.; Ganapathy, V. Cloning and functional characterization of a σ receptor from rat brain. *J. Neurochem.* **1998**, *70*, 922−932.
(5) Kekuda, R.; Prasad, P. D.; Fei, Y.-J.; Leibach, F. H.; Ganapathy, V. Cloning and functional expression of the human type 1 sigma receptor (hSigmaR1). *Biochem. Biophys. Res. Commun.* **1996**, *229*, 553−558.
(6) Aydar, E.; Palmer, C. P.; Klyachko, V. A.; Jackson, M. B. The sigma receptor as a ligand-regulated auxiliary potassium channel subunit. *Neuron* **2002**, *34*, 399−410.
(7) Hayashi, T.; Su, T. P. Sigma-1 receptor ligands: potential in the treatment of neuropsychiatric disorders. *CNS Drugs* **2004**, *18*, 269−284.
(8) Cobos, E. J.; Entrena, J. M.; Nieto, F. R.; Cendan, C. M.; DelPezo, E. Pharmacology and therapeutic potential of sigma$_1$ receptor ligands. *Curr. Pharmacol.* **2008**, *6*, 344−366.
(9) Maurice, T.; Su, T. P. The pharmacology of sigma-1 receptors. *Pharmacol. Ther.* **2009**, *124*, 195−206.
(10) Ishikawa, M.; Hashimoto, K. The role of sigma-1 receptors in the pathophysiology of neuropsychiatric diseases. *J. Recept., Ligand Channel Res.* **2010**, *3*, 25−36.
(11) Choia, S.-R.; Yange, B.; Ploessla, K.; Chumpradita, S.; Weya, S.-P.; Actona, P. D.; Wheelerc, K.; Mach, R. H.; Kunga, H. F. Development of a Tc-99m labeled sigma-2 receptor-specific ligand as a potential breast tumor imaging agent. *Nucl. Med. Biol.* **2001**, *28*, 657−666.
(12) Tu, Z.; Xu, J.; Jones, L. A.; Li, S.; Dumstorff, C.; Vangveravong, S.; Chen, D. L.; Wheeler, K. T.; Welch, M. J.; Mach, R. H. Fluorine-18-labeled benzamide analogues for imaging the σ_2 receptor status of solid tumors with positron emission tomography. *J. Med. Chem.* **2007**, *50*, 3194−3204.
(13) Wilke, R. A.; Lupardus, P. J.; Grandy, D. K.; Rubinstein, M.; Low, M. J.; Jackson, M. B. K^+ channel modulation in rodent neurohypophysial nerve terminals by sigma receptors and not by dopamine receptors. *J. Physiol.* **1999**, *517*, 391−406.
(14) Aydar, E.; Palmer, C. P.; Djamgoz, M. B. A. Sigma receptors and cancer: possible involvement of ion channels. *Cancer Res.* **2004**, *64*, 5029−5035.
(15) Monnet, F. P. Sigma-1 receptor as regulator of neuronal intracellular Ca^{2+}: clinical and therapeutic relevance. *Biol. Cell* **2005**, *97*, 873−883.
(16) Zhang, H.; Cuevas, J. Sigma receptors inhibit high-voltage-activated calcium channels in rat sympathetic and parasympathetic neurons. *J. Neurophysiol.* **2002**, *87*, 2867−2879.
(17) Bermack, J. E.; Debonnel, G. Distinct modulatory roles of sigma receptor subtypes on glutamatergic responses in the dorsal hippocampus. *Synapse* **2005**, *55*, 37−44.
(18) Gudelsky, G. A. Biphasic effect of sigma receptor ligands on the extracellular concentration of dopamine in the striatum of the rat. *J. Neural Transm.* **1999**, *106*, 849−856.
(19) Bowen, W. D. Sigma receptors: recent advances and new clinical potentials. *Pharm. Acta Helv.* **2000**, *74*, 211−218.
(20) Schläger, T.; Schepmann, D.; Würthwein, E.-U.; Wünsch, B. Synthesis and structure-affinity relationships of novel spirocyclic σ receptor ligands with furopyrazole structure. *Bioorg. Med. Chem.* **2008**, *16*, 2992−3001.
(21) Schläger, T.; Schepmann, D.; Lehmkuhl, K.; Holenz, J.; Vela, J. M.; Buschmann, H.; Wünsch, B. Combination of two pharmacophoric systems: synthesis and pharmacological evaluation of spirocyclic pyranopyrazoles with high σ_1 receptor affinity. *J. Med. Chem.* **2011**, *54*, 6704−6713.
(22) Meyer, C.; Neue, B.; Schepmann, D.; Yanagisawa, S.; Yamaguchi, J.; Würthwein, E.-U.; Itami, K.; Wünsch, B. Exploitation of an additional hydrophobic pocket of σ_1 receptors: late-stage diverse modifications of spirocyclic thiophenes by C-H bond functionalization. *Org. Biomol. Chem.* **2011**, *9*, 8016−8029.
(23) Meyer, C.; Schepmann, D.; Yanagisawa, S.; Yamaguchi, J.; Itami, K.; Wünsch, B. Late-stage C-H bond arylation of spirocyclic σ_1 ligands for analysis of complementary σ_1 receptor surface. *Eur. J. Org. Chem.* **2012**, in press.
(24) Oberdorf, C.; Schmidt, T. J.; Wünsch, B. 5D-QSAR for spirocyclic σ_1 receptor ligands by Quasar receptor surface modeling. *Eur. J. Med. Chem.* **2010**, *45*, 3116−3124.
(25) Wünsch, B. Pharmacophore models and development of spirocyclic ligands for σ_1 receptor. *Curr. Pharm. Des.* **2012**, *18*, 930−937.
(26) Hassan, J.; Sévignon, M.; Gozzi, C.; Schulz, E.; Lemaire, M. Aryl−aryl bond formation one century after the discovery of the Ullmann reaction. *Chem. Rev.* **2002**, *102*, 1359−1470.
(27) Oberdorf, C.; Schepmann, D.; Vela, J. M.; Diaz, J. L.; Holenz, J.; Wünsch, B. Thiophene bioisosteres of spirocyclic σ receptor ligands. 1. N-substituted spiro[piperidine-4,4′-thieno[3,2-*c*]pyrans]. *J. Med. Chem.* **2008**, *51*, 6531−6537.
(28) Oberdorf, C.; Schepmann, D.; Vela, J. M.; Buschmann, H.; Holenz, J.; Wünsch, B. Thiophene bioisosters of spirocyclic σ receptor ligands: relationships between substitution pattern and σ receptor affinity. *J. Med. Chem.* **2012**, *55*, 5350−5360.
(29) Ohta, A.; Akita, Y.; Ohkuwa, T.; Chiba, M.; Fukunaga, R.; Miyafuji, A.; Nakata, T.; Tani, N.; Aoyagi, Y. Palladium-catalyzed arylation of furan, thiophene, benzobfuran and benzobthiophene. *Heterocycles* **1990**, *31*, 1951.
(30) Liégault, B.; Lapointe, D.; Caron, L.; Vlassova, A.; Fagnou, K. Establishment of broadly applicable reaction conditions for the palladium-catalyzed direct arylation of heteroatom-containing aromatic compounds. *J. Org. Chem.* **2009**, *74*, 1826−1834.
(31) Yanagisawa, S.; Sudo, T.; Noyori, R.; Itami, K. Direct C-H arylation of (hetero)arenes with aryl iodides via rhodium catalysis. *J. Am. Chem. Soc.* **2006**, *128*, 11748−11749.
(32) Yanagisawa, S.; Sudo, T.; Noyori, R.; Itami, K. Direct coupling of arenes and iodoarenes catalyzed by a rhodium complex with a strongly pi-accepting phosphite ligand. *Tetrahedron* **2008**, *64*, 6073−6081.
(33) Benoît, J.; Yamamoto, T.; Itami, K. Iridium catalysis for C−H bond arylation of heteroarenes with iodoarenes. *Angew. Chem., Int. Ed.* **2009**, *48*, 3644−3647.
(34) Do, H.-Q.; Khan, R. M. K.; Daugulis, O. A general method for copper-catalyzed arylation of arene C−H bonds. *J. Am. Chem. Soc.* **2008**, *130*, 15185−15192.
(35) Yanagisawa, S.; Itami, K. Palladium/2,2′-bipyridyl/Ag_2CO_3 catalyst for C−H bond arylation of heteroarenes with haloarenes. *Tetrahedron* **2011**, *67*, 4425−4430.
(36) Yanagisawa, S.; Ueda, K.; Sekizawa, H.; Itami, K. Programmed synthesis of tetraarylthiophenes through sequential C-H arylation. *J. Am. Chem. Soc.* **2009**, *131*, 14622−14623.
(37) Ueda, K.; Yanagisawa, S.; Yamaguchi, J.; Itami, K. A general catalyst for the β-selective C−H bond arylation of thiophenes with iodoarenes. *Angew. Chem., Int. Ed.* **2010**, *49*, 8946−8949.
(38) Kirchberg, S.; Tani, S.; Ueda, K.; Yamaguchi, J.; Studer, A.; Itami, K. Oxidative biaryl coupling of thiophenes and thiazoles with arylboronic acids through palladium catalysis: otherwise difficult C4-selective C-H arylation enabled by boronic acids. *Angew. Chem., Int. Ed.* **2011**, *50*, 2387−2391.
(39) Maier, C. A.; Wünsch, B. Novel spiropiperidines as highly potent and subtype selective σ-receptor ligands. Part 1. *J. Med. Chem.* **2002**, *45*, 438−448.
(40) Maier, C. A.; Wünsch, B. Novel σ receptor ligands. Part 2. SAR of spiro[[2]benzopyran-1,4′-piperidines] and spiro[[2]benzofuran-1,4′-piperidines] with carbon substituents in position 3. *J. Med. Chem.* **2002**, *45*, 4923−4930.
(41) Große Maestrup, E.; Wiese, C.; Schepmann, D.; Hiller, A.; Fischer, S.; Scheunemann, M.; Brust, P.; Wünsch, B. Synthesis of spirocyclic σ_1 receptor ligands as potential PET radiotracers, structure-affinity relationships and in vitro metabolic stability. *Bioorg. Med. Chem.* **2009**, *17*, 3630−3641.
(42) Holl, R.; Schepmann, D.; Fröhlich, R.; Grünert, R.; Bednarski, P. J.; Wünsch, B. Dancing of the second aromatic residue around the 6,8-diazabicyclo[3.2.2]-nonane framework: influence on σ receptor affinity and cytotoxicity. *J. Med. Chem.* **2009**, *52*, 2126−2137.

(43) Wiese, C.; Große Maestrup, E.; Schepmann, D.; Vela, J. M.; Holenz, J.; Buschmann, H.; Wünsch, B. Pharmacological and metabolic characterisation of the potent σ_1 receptor ligand 1′-benzyl-3-methoxy-3*H*-spiro[[2]benzofuran-1,4′-piperidine]. *J. Pharm. Pharmacol.* **2009**, *61*, 631−640.
(44) Wirt, U.; Schepmann, D.; Wünsch, B. Asymmetric synthesis of 1-substituted tetrahydro-3-benzazepines as NMDA receptor antagonists. *Eur. J. Org. Chem.* **2007**, 462−475.
(45) Schepmann, D.; Frehland, B.; Lehmkuhl, K.; Tewes, B.; Wünsch, B. Development of a selective competitive receptor binding assay for the determination of the affinity to NR2B containing NMDA receptors. *J. Pharm. Biomed. Anal.* **2010**, *53*, 603−608.
(46) Li, H.; Sutter, J.; Hoffman, R. HypoGen: An automated system for generating 3D predictive pharmacophore models. In *Pharmacophore Perception, Development, and Use in Drug Design*; Guner, O. F., Ed.; International University Line: La Jolla, CA, 1999; pp 173−189.
(47) Sutter, J.; Guner, O. F.; Hoffman, R. D.; Li, H.; Wadman, M. Effect of variable weight and tolerances on predictive model generation. In *Pharmacophore Perception, development, and Use in Drug Design*; Guner, O. F., Ed.; International University Line: La Jolla, CA, 1999; pp 501−511.
(48) Glennon, R. A.; Ablordeppey, S. Y.; Ismaiel, A. M.; El-Ashmawy, M. B.; Fischer, J. B.; Howie, K. B. Structural features important for σ_1 receptor binding. *J. Med. Chem.* **1994**, *37*, 1214−19.
(49) Laggner, C.; Schieferer, C.; Fiechtner, B.; Poles, G.; Hoffmann, R. D.; GLossmann, H.; Langer, T.; Moebius, F. Discovery of high-affinity ligands of σ_1 receptor, ERG2, and emopamil binding protein by pharmacophore modeling and virtual screening. *J. Med. Chem.* **2005**, *48*, 4754−4764.
(50) Laurini, E.; Dal Col, V.; Mamolo, M. G.; Zampieri, D.; Posocco, P.; Fermeglia, M.; Vio, L.; Pricl, S. Homology model and docking-based virtual screening for ligands of the σ1 receptor. *ACS Med. Chem. Lett.* **2011**, *2*, 834−839.
(51) Zampieri, D.; Mamolo, M. G.; Laurini, E.; Florio, C.; Zanette, C.; Fermeglia, M.; Posocco, P.; Paneni, M. S.; Pricl, S.; Vio, L. Synthesis, biological evaluation, and three-dimensional *in silico* pharmacophore model for σ1 receptor ligands based on a series of substituted benzo[*d*]oxazol-2(3*H*)-one derivatives. *J. Med. Chem.* **2009**, *52*, 5380−5393.
(52) Seth, P.; Ganapathy, M. E.; Conway, S. J.; Bridges, C. D.; Smith, S. B.; Casellas, P.; Ganapathy, V. Expression pattern of the type 1 sigma receptor in the brain and identity of critical anionic amino acid residues in the ligand-binding domain of the receptor. *Biochim. Biophys. Acta* **2001**, *1540*, 59−67.
(53) Pal, A.; Fontanilla, A. R.; Ramachandran, S.; Chu, U. B.; Mavlyutov, T.; Ruoho, A. E. Identification of regions of the sigma-1 receptor ligand binding site using a novel photoprobe. *Mol. Pharmacol.* **2007**, *72*, 921−933.
(54) Pal, A.; Chu, U. B.; Ramachandran, S.; Grawoig, D.; Guo, L. W.; Hajipour, A. R.; Ruoho, A. E. Juxtaposition of the steroid binding domain-like I and II regions constitutes a ligand binding site in the σ-1 receptor. *J. Biol. Chem.* **2008**, *283*, 19646−19656.
(55) Srinivasan, J.; Cheatham, T. E., III; Cieplak, P.; Kollman, P. A.; Case, D. A. Continuum solvent studies of the stability of DNA, RNA, and phosphoramidate−DNA helices. *J. Am. Chem. Soc.* **1998**, *120*, 9401−9409.
(56) For a selected list of recent, successful applications of the MM/PBSA methodology in related topics from our group see, for instance: (a) Carta, A.; Briguglio, I.; Piras, S.; Boatto, G.; La Colla, P.; Loddo, R.; Tolomeo, M.; Grimaudo, S.; Di Cristina, A.; Pipitone, R. M.; Laurini, E.; Paneni, M. S.; Posocco, P.; Fermeglia, M.; Pricl, S. 3-Aryl-2-[1H-benzotriazol-1-yl]acrylonitriles: a novel class of potent tubulin inhibitors. *Eur. J. Med. Chem.* **2011**, *46*, 4151−4167. (b) Liu, X.; Chen, H.; Laurini, E.; Wang, Y.; Dal Col, V.; Posocco, P.; Ziarelli, F.; Fermeglia, M.; Zhang, C. C.; Pricl, S.; Peng, L. 2-Difluoromethylene-4-methylenepentanoic acid, a paradoxical probe able to mimic the signaling role of 2-oxoglutaric acid in cyanobacteria. *Org. Lett.* **2011**, *13*, 2924−2927. (c) Giliberti, G.; Ibba, C.; Marongiu, E.; Loddo, R.; Tonelli, M.; Boido, V.; Laurini, E.; Posocco, P.; Fermeglia, M.; Pricl, S. Synergistic experimental/computational studies on arylazoenamine derivatives that target the bovine viral diarrhea virus RNA-dependent RNA polymerase. *Bioorg. Med. Chem.* **2010**, *18*, 6055−6068. (d) Tonelli, M.; Boido, V.; La Colla, P.; Loddo, R.; Posocco, P.; Paneni, M. S.; Fermeglia, M.; Pricl, S. Pharmacophore modeling, resistant mutant isolation, docking, and MM-PBSA analysis: combined experimental/computer-assisted approaches to identify new inhibitors of the bovine viral diarrhea virus (BVDV). *Bioorg. Med. Chem.* **2010**, *18*, 2304−2316. (e) Carta, A.; Pricl, S.; Piras, S.; Fermeglia, M.; La Colla, P.; Loddo, R. Activity and molecular modeling of a new small molecule active against NNRTI-resistant HIV-1 mutants. *Eur. J. Med. Chem.* **2009**, *44*, 5117−5122. (f) Tonelli, M.; Vazzana, I.; Tasso, B.; Boido, V.; Sparatore, F.; Fermeglia, M.; Paneni, M. S.; Posocco, P.; Pricl, S.; La Colla, P.; Ibba, C.; Secci, B.; Collu, G.; Loddo, R. Antiviral and cytotoxic activities of aminoarylazo compounds and aryltriazene derivatives. *Bioorg. Med. Chem.* **2009**, *17*, 4425−4440 and references therein.
(57) Brooks, B. R.; Bruccoleri, R. E.; Olafson, B. D.; States, D. J.; Swaminathan, S.; Karplus, M. J. CHARMM: a program for macromolecular energy, minimization, and dynamics calculations. *J. Comput. Chem.* **1983**, *4*, 187−217.
(58) (a) Smellie, A.; Teig, S. L.; Towbin, P. Poling: promoting conformational variation. *J. Comput. Chem.* **1994**, *16*, 171−187. (b) Smellie, A.; Kahn, S. D.; Teig, S. L. Analysis of conformational coverage. 1. Validation and estimation of coverage. *J. Chem. Inf. Comput. Sci.* **1995**, *35*, 285−294. (c) Smellie, A.; Kahn, S. D.; Teig, S. L. Analysis of conformational coverage. 2. Applications of conformational models. *J. Chem. Inf. Comput. Sci.* **1995**, *35*, 295−304.
(59) Fisher, R. *The Design of Experiments*; Hafner Publishing: New York, 1966.
(60) (a) Laurini, E.; Zampieri, D.; Mamolo, M. G.; Vio, L.; Zanette, C.; Florio, C.; Posocco, P.; Fermeglia, M.; Pricl, S. A 3D-pharmacophore model for sigma2 receptors based on a series of substituted benzo[d]oxazol-2(3H)-one derivatives. *Bioorg. Med. Chem. Lett.* **2010**, *20*, 2954−2957. (b) Mazzei, M.; Nieddu, E.; Miele, M.; Balbi, A.; Ferrone, M.; Fermeglia, M.; Mazzei, M. T.; Pricl, S.; La Colla, P.; Marongiu, F.; Ibba, C.; Loddo, R. Activity of Mannich bases of 7-hydroxycoumarin against Flaviviridae. *Bioorg. Med. Chem.* **2008**, *16*, 2591−2605. (c) Zampieri, D.; Mamolo, M. G.; Vio, L.; Banfi, E.; Scialino, G.; Fermeglia, M.; Ferrone, M.; Pricl, S. Synthesis, antifungal and antimycobacterial activities of new bis-imidazole derivatives, and prediction of their binding to P450(14DM) by molecular docking and MM/PBSA method. *Bioorg. Med. Chem.* **2007**, *15*, 7444−7458. (d) Carta, A.; Loriga, M.; Paglietti, G.; Ferrone, M.; Fermeglia, M.; Pricl, S.; Sanna, T.; Ibba, C.; La Colla, P.; Loddo, R. Design, synthesis, and preliminary *in vitro* and *in silico* antiviral activity of [4,7]-phenantrolines and 1-oxo-1,4-dihydro-[4,7]phenantrolines against single-stranded positive-sense RNA genome viruses. *Bioorg. Med. Chem.* **2007**, *15*, 1914−1927. (e) Carta, A.; Loriga, G.; Piras, S.; Paglietti, G.; Ferrone, M.; Fermeglia, M.; Pricl, S.; La Colla, P.; Secci, B.; Collu, G.; Loddo, R. Synthesis and *in vitro* evaluation of the antiviral activity of N-[4-(1H(2H)-benzotriazol-1(2)-yl)phenyl]-alkylcarboxamides. *Med. Chem.* **2006**, *2*, 577−589. (f) Frecer, V.; Kabeláč, M.; De Nardi, P.; Pricl, S.; Miertuš, S. Structure-based design of inhibitors of NS3 serine protease of hepatitis C virus. *J. Mol. Graphics Modell.* **2004**, *22*, 209−220. (g) Felluga, F.; Pitacco, G.; Valentin, E.; Coslanich, A.; Fermeglia, M.; Ferrone, M.; Pricl, S. studying enzyme enantioselectivity using combined *ab initio* and free energy calculations: α-chymotrypsin and methyl cis- and trans-5-oxo-2-pentylpirrolidine-3-carboxylates. *Tetrahedron: Asymmetry* **2003**, *14*, 3385−3399.
(61) Case, D. A.; Darden, T. A.; Cheatham, T. E., III; Simmerling, C. L.; Wang, J.; Duke, R. E.; Luo, R.; Walker, R. C.; Zhang, W.; Merz, K. M.; Roberts, B.; Wang, B.; Hayik, S.; Roitberg, A.; Seabra, G.; Kolossváry, I.; Wong, K. F.; Paesani, F.; Vanicek, J.; Wu, X.; Brozell, S. R.; Steinbrecher, T.; Gohlke, H.; Cai, Q.; Ye, X.; Wang, J.; Hsieh, M.-J.; Cui, G.; Roe, D. R.; Mathews, D. H.; Seetin, M. G.; Sagui, C.; Babin, V.; Luchko, T.; Gusarov, S.; Kovalenko, A.; Kollman, P. A. *AMBER 11*; University of California: San Francisco, CA, 2010.

(62) (a) Bayly, C. I.; Cieplak, P.; Cornell, W. D.; Kollman, P. A. A well-behaved electrostatic potential based method using charge restraints for determining atom-centered charges: the RESP model. *J. Phys. Chem.* **1993**, *97*, 10269−10280. (b) Cornell, W. D.; Cieplak, P.; Bayly, C. I.; Kollman, P. A. Application of RESP charges to calculate conformational energies, hydrogen bond energies and free energies of solvation. *J. Am. Chem. Soc.* **1993**, *115*, 9620−9631. (c) Cieplak, P.; Cornell, W. D.; Bayly, C. I.; Kollman, P. A. Application of the multimolecule and multiconformational RESP methodology to biopolymers: charge derivation for DNA, RNA and proteins. *J. Comput. Chem.* **1995**, *16*, 1357−1377.

(63) Singh, U. C.; Kollman, P. A. An approach to computing electrostatic charges for molecules. *J. Comput. Chem.* **1984**, *5*, 129−145.

(64) Besler, B. H.; Merz, K. M.; Kollman, P. A. Atomic charges derived from semiempirical methods. *J. Comput. Chem.* **1990**, *11*, 431−439.

(65) Duan, Y.; Wu, C.; Chowdhury, S.; Lee, M. C.; Xiong, G.; Zhang, W.; Yang, R.; Cieplak, P.; Luo, R.; Lee, T.; Caldwell, J.; Wang, J.; Kollman, P. A. Point-charge force field for molecular mechanics simulations of proteins based on condensed-phase quantum mechanical calculations. *J. Comput. Chem.* **2003**, *24*, 1999−2012.

(66) Wang, J.; Wolf, R. M.; Caldwell, J. W.; Kollman, P. A.; Case, D. A. Development and testing of a general amber force field. *J. Comput. Chem.* **2004**, *25*, 1157−1174.

(67) Morris, G. M.; Huey, R.; Lindstrom, W.; Sanner, M. F.; Belew, R. K.; Goodsell, D. S.; Olson, A. J. AutoDock4 and AutoDockTools4: automated docking with selective receptor flexibility. *J. Comput. Chem.* **2009**, *30*, 2785−2791.

(68) Mehler, E. L.; Solmajer, T. Electrostatic effects in proteins: comparison of dielectric and charge models. *Protein Eng.* **1991**, *4*, 903−910.

(69) (a) Onufriev, A.; Bashford, D.; Case, D. A. Modification of the generalized Born model suitable for macromolecules. *J. Phys. Chem. B* **2000**, *104*, 3712−3720. (b) Feig, M.; Onufriev, A.; Lee, M. S.; Im, W.; Case, D. A.; Brooks, C. L. Performance comparison of generalized Born and Poisson methods in the calculation of electrostatic solvation energies for protein structures. *J. Comput. Chem.* **2004**, *25*, 265−284.

(70) Jorgensen, W. L.; Chandrasekhar, J.; Madura, J. D.; Impey, R. W.; Klein, M. L. Comparison of simple potential functions for simulating liquid water. *J. Chem. Phys.* **1983**, *79*, 926−935.

(71) Ryckaert, J.-P.; Ciccotti, G.; Berendsen, H. J. C. Numerical integration of the cartesian equations of motion of a system with constraints: molecular dynamics of n-alkanes. *J. Comput. Phys.* **1977**, *23*, 327−341.

(72) Toukmaji, A.; Sagui, C.; Board, J.; Darden, T. Efficient particle-mesh Ewald based approach to fixed and induced dipolar interactions. *J. Chem. Phys.* **2000**, *113*, 10913−10927.

(73) For a further selection of successful MM/PBSA applications in ligand binding of our group see also: (a) Liu, X.; Liu, C.; Laurini, E.; Posocco, P.; Pricl, S.; Qu, F.; Rocchi, P.; Peng, L. Efficient delivery of sticky siRNA and potent gene silencing in a prostate cancer model using a generation 5 triethanolamine-core PAMAM dendrimer. *Mol. Pharm.* **2012**, *9*, 470−481. (b) Karatasos, K.; Posocco, P.; Laurini, E.; Pricl, S. Poly(amidoamine)-based dendrimer/siRNA complexation studied by computer simulations: effects of pH and generation on dendrimer structure and siRNA binding. *Macromol. Biosci.* **2012**, *12*, 225−240. (c) Liu, X.; Wu, J.; Yammine, M.; Zhou, J.; Posocco, P.; Viel, S.; Liu, C.; Ziarelli, F.; Fermeglia, M.; Pricl, S.; Victorero, G.; Nguyen, C.; Erbacher, P.; Behr, J. P.; Peng, L. Structurally flexible triethanolamine core PAMAM dendrimers are effective nanovectors for DNA transfection *in vitro* and *in vivo* to the mouse thymus. *Bioconjugate Chem.* **2011**, *22*, 2461−7243. (d) Barnard, A.; Posocco, P.; Pricl, S.; Calderon, M.; Haag, R.; Hwang, M. E.; Shum, V. W.; Pack, D. W.; Smith, D. K. Degradable self-assembling dendrons for gene delivery: experimental and theoretical insights into the barriers to cellular uptake. *J. Am. Chem. Soc.* **2011**, *133*, 20288−20300. (e) Pierotti, M. A.; Tamborini, E.; Negri, T.; Pricl, S.; Pilotti, S. Targeted therapy in GIST: *in silico* modeling for prediction of resistance. *Nat. Rev. Clin. Oncol.* **2011**, *8*, 161−170. (f) Pavan, G. M.; Posocco, P.; Tagliabue, A.; Maly, M.; Malek, A.; Danani, A.; Ragg, E.; Catapano, C. V.; Pricl, S. PAMAM dendrimers for siRNA delivery: computational and experimental insights. *Chem.—Eur. J.* **2010**, *16*, 7781−7795. (g) Dileo, P.; Pricl, S.; Tamborini, E.; Negri, T.; Stacchiotti, S.; Gronchi, A.; Posocco, P.; Laurini, E.; Coco, P.; Fumagalli, E.; Casali, P. G.; Pilotti, S. Imatinib response in two GIST patients carrying two hitherto functionally uncharacterized PDGFRA mutations: an imaging, biochemical and molecular modeling study. *Int. J. Cancer* **2011**, *128*, 983−990. (h) Jones, S. P.; Pavan, G. M.; Danani, A.; Pricl, S.; Smith, D. K. Quantifying the effect of surface ligands on dendron-DNA interactions: insights into multivalency through a combined experimental and theoretical approach. *Chem.—Eur. J.* **2010**, *16*, 4519−4532. (i) Pierotti, M. A.; Negri, T.; Tamborini, E.; Perrone, F.; Pricl, S.; Pilotti, S. Targeted therapies: the rare cancer paradigm. *Mol. Oncol.* **2010**, *4*, 19−37. (j) Conca, E.; Negri, T.; Gronchi, A.; Fumagalli, E.; Tamborini, E.; Pavan, G. M.; Fermeglia, M.; Pierotti, M. A.; Pricl, S.; Pilotti, S. Activate and resist: L576P-KIT in GIST. *Mol. Cancer Ther.* **2009**, *8*, 2491−2495. (k) Woodman, S. E.; Trent, J. C.; Stemke-Hale, K.; Lazar, A. J.; Pricl, S.; Pavan, G. M.; Fermeglia, M.; Gopal, Y. N.; Yang, D.; Podoloff, D. A.; Ivan, D.; Kim, K. B.; Papadopoulos, N.; Hwu, P.; Mills, G. B.; Davies, M. A. Activity of dasatinib against L576P KIT mutant melanoma: molecular, cellular, and clinical correlates. *Mol. Cancer Ther.* **2009**, *8*, 2079−2085. (l) Pavan, G. M.; Danani, A.; Pricl, S.; Smith, D. K. Modeling the multivalent recognition between dendritic molecules and DNA: understanding how ligand "sacrifice" and screening can enhance binding. *J. Am. Chem. Soc.* **2009**, *131*, 9686−9694 and references therein.

(74) Gilson, M. K.; Sharp, K. A.; Honig, B. H. Calculating the electrostatic potential of molecules in solution: method and error assessment. *J. Comput. Chem.* **1988**, *9*, 327−335.

(75) Sitkoff, D.; Sharp, K. A.; Honig, B. Accurate calculation of hydration free energies using macroscopic solvent models. *J. Phys. Chem.* **1994**, *98*, 1978−1988.

(76) Sanner, M. F.; Olson, A. J.; Spehner, J. C. Reduced surface: an efficient way to compute molecular surfaces. *Biopolymers* **1996**, *38*, 305−320.

(77) Wilson, E. B., Decius, J. C., Cross, P. C. *Molecular Vibrations*; McGraw-Hill: New York, 1995.

(78) http://www.esteco.com/home/mode_frontier/mode_frontier.html.